Active normal faulting and the seismogenic fault of the 1739 M 8.0 Pingluo earthquake in the intracontinental Yinchuan Graben, China

Lin, Aiming; Hu, Jianmin; Gong, Wangbin

(Red color indicating the main revisions)

Active normal faulting and the seismogenic fault of the 1739 M ~8.0 Pingluo earthquake in the intracontinental Yinchuan Graben, China

Aiming Lin[1]*, Jianmin Hu[2], and Wangbin Gong[2]

[1]Department of Geophysics, Graduate School of Science,

Kyoto University, Kyoto 606-8502, Japan

[2]Institute of Geomechanics, Chinese Academy of Geological Sciences,

Beijing 100081, China

***Corresponding author:**
Department of Geophysics
Graduate School of Science
Kyoto University
606-8502 Kyoto
Japan
E-mail: slin@kugi.kyoto-u.ac.jp

Abstract:

The NNE-trending Yinchuan Graben is one of several intracontinental grabens that have developed in the extensional environment around the Ordos Block, northern-central China, and is bounded by active normal faults at both its eastern and western margins. In this study, we present new evidence for the Holocene activity and paleoseimicity of the active normal faults developed in the Yinchuan Graben. Interpretations of high-resolution WorldView and Google images, field investigations, trench excavations, seismic data, and radiocarbon dating results reveal the following: i) two main active fault zones, the Helanshan Piedmont Fault Zone (HPFZ) along the western margin of the graben and the Huanghe Fault (HHF) along the eastern margin, are characterized by conspicuous fault scarps developed on both Holocene alluvial fans and terrace risers; ii) the active faults are dominated by normal faulting; iii) the Holocene normal slip rate is estimated to be ~2–3 mm/yr, and the recurrence interval of morphogenic earthquakes is estimated to be ~1500–2000 yr for both the HPFZ and HHF; and iv) the HHF is the most likely seismogenic fault for the triggering of the 1739 M

~8.0 Pingluo earthquake. Our results show that the HPFZ has the potential to produce a destructive earthquake in the near future, because no large earthquake has occurred on this fault during the past ~1500 years. This contrasts with previous findings that the fault scarps of the HPFZ were caused by the 1739 Pingluo earthquake and that therefore the likelihood of a large and destructive earthquake on that fault in the near future is relatively small because of the <300 years elapsed since the earthquake. Therefore, it is necessary to reconstruct the model of faulting, tectonic activity, and paleoseismicity of the intracontinental graben and to reassess the seismic hazard of the active normal faults for the densely populated Yinchuan region.

Keywords: active normal fault, Yinchuan Graben, 1739 M ~8.0 Pingluo earthquake, Helanshan Piedmont Fault Zone, Huanghe Fault, Ordos Block

1. Introduction

Active normal faults generally occur in places where the crust is being stretched under an extensional regime (e.g., Jackson, 1987; Jackson and White, 1989; Yeats et al., 1997; Rao et al., 2014). The Yinchuan Graben is one of several intracontinental tectonic grabens in which many active normal faults have developed in the extensional regime around the Ordos Block in northern-central China (Figure 1). Therefore, investigating the activity and kinematic characteristics of active normal faults in the Yinchuan Graben should provide a better understanding of the seismotectonic features and tectonic evolution of active extensional grabens around the Ordos Block. The Yinchuan Graben has long attracted research attention on account of its high levels of historical paleoseismicity and its normal faulting regime sustained since the early Eocene (Liao and Pan, 1982; Liao et al., 1982; Li and Wan, 1984; Zhang et al., 1986; Deng and Liao, 1996; Zhao et al., 2007; Fang et al., 2009; Feng et al., 2011).

A marked offset of the Great Wall of China, which was built at the northern end of the graben in AD 1531, is considered to have been produced by

67 the 1739 M ~8.0 Pingluo earthquake along the Helanshan Piedmont Fault Zone
68 (HPFZ), which is developed along the western margin of the Yinchuan Graben
69 (He, 1982; Liao and Pan, 1982; Deng et al., 1984; Zhang et al., 1986; Deng and
70 Liao, 1996); that is, the HPFZ is considered to have been the source seismogenic
71 fault of the 1739 earthquake. Furthermore, the morphologic evolution of fault
72 scarps, and paleoseismicity including the recurrence intervals and slip rates of
73 large earthquakes, have been documented for the HPFZ based mainly on the
74 proposal that the fault scarps of the HPFZ are associated with 1739 earthquake
75 (e.g., Zhang et al., 1986; Deng and Liao, 1996).

76 However, our recent fieldwork has demonstrated that the Great Wall was
77 not offset by the M ~8.0 Pingluo earthquake of 1739 as reported previously, but
78 was actually built on preexisting active fault scarps, and that the 1739 earthquake
79 was not triggered by the HPFZ (Lin et al., 2013). Therefore, it is necessary to
80 reevaluate the current activity of active normal faults in the graben and to
81 re-identify the source seismogenic fault that triggered the 1739 M ~8.0 Pingluo
82 earthquake in order to assess the seismic hazard in the densely populated

Yinchuan region. In this study, we present new evidence demonstrating the Holocene activity of the active normal faults developed in the Yinchuan Graben and discuss the paleoseismicity, including the 1739 M ~8.0 Pingluo earthquake.

2. Tectonic setting

The study area, the Yinchuan Graben, is located on the western side of the Ordos Block, northern-central China. The graben is bounded by the NNE-trending Helan Mountains to the west and the NNE-flowing Huanghe (*Yellow River* in English) to the east, and is ~150 km long and 50–55 km wide (Fig. 1). Geologic evidence and seismic reflection data show that the graben contains more than 7000 m of Tertiary sediments and ~1200–1400 m of unconsolidated Quaternary sediments, indicating a long period of subsidence in an extensional tectonic environment (Feng et al., 2011). The basement consists of pre-Cenozoic metamorphic rocks (Figure 1b). The main active faults in the graben strike NNE–SSW, parallel to the orientation of graben, and include (from east to west) the Huanghe (HH), Yinchuan–Pingluo, Luhuatai, and Helanshan

99 Piedmont (HP) faults (Fig.1b). Seismic reflection data show that the HHFZ,
100 which runs along the eastern margin of the Helan Mountains, is the main fault
101 forming the western boundary of the graben (Fig. 1b and c; Fang et al., 2009;
102 Feng et al., 2011). The Huanghe Fault (HHF), along which the Yellow River
103 flows to the NNE, is inferred to be a blind fault and its recent activity is unclear
104 (Deng and Liao, 1996). The Yinchuan–Pingluo and Luhuatai faults are inferred
105 faults for which there is no morphotectonic evidence, and therefore their current
106 activity is also unknown (Zhang et al., 1986; Deng and Liao, 1996). The HPFZ is
107 considered to be a major active normal fault zone with a dextral displacement
108 component, and is thought to be the source seismogenic fault of the 1739 M ~8.0
109 Pingluo earthquake, based on the apparent offset of the Great Wall (He, 1982;
110 Liao and Pan, 1982; Zhang et al., 1982; Deng et al., 1984; Deng and You, 1985;
111 Zhang et al., 1986; Deng and Liao, 1996). The average recurrence interval of
112 destructive earthquakes on the HHFZ has been estimated to be thousands of
113 years to ten thousand years (Zhang et al., 1986) or ~2300–3000 yr (Deng and
114 Liao, 1996).

115 Historical records show that four large (M > 6) earthquakes, the 1143 M
116 6.5, 1471 M 6.5, 1921 M 6.0, and 1739 M ~8.0 Pingluo earthquakes, have
117 occurred in the Yinchuan Graben during the last millennium (Zhang et al., 1986;
118 People Network, 2014). The 1739 M ~8.0 Pingluo earthquake occurred on 3
119 January 1739 and caused more than 50,000 deaths (Zhang et al., 1986; Bai et al.,
120 2005; People Network, 2014). Based on the damage and ground deformation
121 features recorded in historical documents, the strongest ground motion caused by
122 this earthquake was concentrated in a narrow zone around the Huanghe and
123 Yinchuan–Pingluo faults on the eastern side of the Yinchuan Graben, where
124 seismic intensities of up to X–XI (on the Chinese XII-point seismic intensity
125 scale) have been estimated (Fig. 1b).
126
127 **3. Study methods**
128 To detect and identify tectonic topographical features associated with the
129 active faults in the study area, we processed perspective remote-sensing images
130 by draping over the high-resolution WorldView over the digital elevation model

(DEM) data and Google images (Figs 2–6). This method made it possible to identify tectono-topographical features, including fault scarps, in the study area. The active fault traces identified using this method were confirmed in the field by detailed mapping, measurements of topographical profiles, trench investigations, and the excavation of fault outcrops (Figs 2c and d, 3b–d, 5c and d, and 6a). To observe fault-zone structures, we also followed fault outcrops along fault traces identified from the images and from topographical features in the field. In representative outcrops, we excavated and cleaned the fault outcrop exposures and then sketched the structural features in detail, as also done for trenching.

To determine the ages of topographical surfaces and alluvial deposits that have been offset and deformed by faulting, we collected carbonate materials from the unconsolidated deposits of both alluvial fans and terrace risers. A total of 25 radiocarbon dating samples were taken from the alluvial deposits and were analyzed at Beta Analytic Inc. USA using accelerator mass spectrometry. Dendrochronologically calibrated calendar ages were obtained following Stuvier

et al. (2003). Radiocarbon dating results and calibrated ages are listed in Table 1.

To measure the amount of offset and to evaluate the recent activity of the active faults in the study area, we divided the alluvial surfaces, including the terrace risers and alluvial fan surfaces used as surface deformation markers, into four levels: T0 (lowermost surface), T1 (lower surface), T2 (middle surface), and T3 (high surface), based on their distribution, continuity, and height from the current channel (Figs 3a–c, 4, and 5a–c). The T0 surface is the lowermost surface and is developed within the current river channels as sand dunes. The T1 surface is the lower surface and is bounded mainly by the current river channels. The T2 surface is widely developed on the alluvial fans across a zone extending for ~10 km and is bounded by the eastern piedmont area of the Helan Mountains. The T3 surface is limited to the narrow areas at the heads of alluvial fans and is bounded by the Helan Mountains piedmont. Radiocarbon dating results of carbonate materials contained in the alluvial deposits show that the T0, T1, T2, and T3 alluvial surfaces formed at <~1000, ~1000–2000, ~2000–8000, and ~8000–12,000 yr BP, respectively (Table 1, Figs 3–6), suggesting that these

alluvial surfaces formed during the period of global warming that started at 12–13 ka (e.g., Fairbanks, 1990; Lehman and Keigwin, 1992). During the fieldwork, we made in-situ measurements of the topographical profiles across the fault scarps developed on both the alluvial fans and terrace risers, and calculated the amounts of vertical offset (Table 2), details of which are described below.

4. Structural features of active faults

4.1. Identification of active faults

On the basis of analytic results of the topographical features and the fault deformation structures, we identified two main active fault zones in the Yinchuan Graben: the Helanshan Piedmont and Huanghe fault zones, which are developed along the western and eastern margins of the graben, respectively (Figure 1b). Previous studies have identified two other inferred faults in the graben: the Luhuatai and Yinchuan–Pingluo faults, identified using seismic reflection data (Fig. 1b and c; Cai et al., 2006; Wang et al., 2007; Fang et al., 2009; Feng et al., 2011; Yang et al., 2011). However, the topographical analysis and field

investigations of the present study show no conspicuous topographical or geologic evidence for tectonic deformation features on the alluvial surfaces, including the terrace risers and alluvial fans, which formed during the Holocene along the Luhuatai and Yinchuan–Pingluo faults (Fig. 1b). On the basis of the lack of both topographical features and geologic deformation structures, we suggest that the Luhuatai and Yinchuan–Pingluo faults are blind faults but have been morphogenically inactive during the Holocene (see Discussion for details). Therefore, there are only two main morphogenic active fault zones in the Yinchuan Graben: the Helanshan Piedmont (HP) and Huanghe (HH) fault zones. The topographical and fault structural features of these two fault zones are described below.

4.2. Topographical features

4.2.1. The Helanshan Piedmont Fault Zone (HPFZ)

Topographically, the HPFZ is characterized by conspicuous fault scarps developed along the topographical boundary between the NNE-trending Helan

Mountains and the Yinchuan Graben (Fig. 1b). The HPFZ is composed of two main faults: the Helanshan Piedmont and Suyukou faults. The Helanshan Piedmont Fault (HPF) is ~130 km long, which is developed along the piedmont of the Helan Mountains, and generally shows irregular and discontinuous traces that are concentrated in a zone ranging from several meters to 500 m wide (Figures 1, and 3–5). In the northeastern part of the graben, in the vicinity of the Great Wall, the fault zone is composed of three subfaults that form a small graben structure (Figure 5) where the Great Wall has been recently demonstrated to be built on the fault scarps (Lin et al., 2013) but not offset by the 1739 M ~8.0 Pingluo earthquake as reported previously by Zhang et al. (1986) and Deng et al. (1996).

In contrast, the Suyukou Fault (SYF), which lies 5 km east of the HPF, extends for only ~18 km and generally shows a continuous fault trace along alluvial fans, easily recognized as conspicuous white-gray lineaments in the high-resolution WorldView and Google images (Figure 2a–c). The fault scarp along the SYF shows a conspicuous shape with a fresh surface facing southeast

211 (Fig. 2d and e), similar to the surfaces of coseismic fault scarps produced by the
212 2008 M_w 7.9 Wenchuan earthquake (Lin et al., 2009, 2010).

213 The HPF offsets the T1, T2, and T3 alluvial surfaces (Figures 3 and 4), for
214 which the amounts of vertical offset calculated from the topographical profiles
215 measured in situ range from 0.6 to 1.4 m, 3.2 to 6.1 m, and 14.3 to 22 m,
216 respectively (Table 2; Figures 3–5). In contrast, the SYF offsets surfaces T1 and
217 T2, for which the amounts of vertical offset range from 1.4 to 2.5 m and 3.2 to
218 11.2 m, respectively (Table 2; Figure 2), similar to the values measured along the
219 HPF. These results indicate that the older the alluvial surface, the larger the
220 amount of offset, demonstrating an accumulation of vertical displacement over
221 time on the surface features cut by the fault scarps.

222

223 **4.2.2. The Huanghe Fault (HHF)**

224 The HHF is developed at the eastern margin of the Yinchuan Graben,
225 where it extends for >120 km and is bounded by the Ordos Block to the east
226 (Figure 1b). The fault runs mainly along or near the Yellow River channel in the

study area, but in the southern part it is mostly covered by desert dunes on the Ordos Block and is difficult to observe in the field. Only in the central part, along the western margin of the Ordos Block, the HHF can be observed in the field (Figs 1b and 6), where terrace risers are developed along the eastern side of the Yellow River (Fig. 6a–c). The terrace risers can be divided into three levels: the lower (T1), middle (T2), and high (T3) terraces based on their distribution and height above the channel of the Yellow River (Fig. 6c and d). The T1 surface is bounded by the Yellow River channel, T2 is limited to a narrow belt parallel to the fault scarp of the HHF, and T3 is bounded by the western edge of the Ordos Block. The fault scarp along the fault has been eroded in many parts and is intact only locally (Fig. 6c). The topographical profiles measured in situ show that the amount of vertical offset is 9–11 m on T2 and >16 m on T3, because the fault scarp has been eroded on T2, and T3 has been covered by younger alluvial deposits on the downthrown (western) side of the HHF (Fig. 6b–d).

4.3. Structural features of the fault deformation zone

243 In this study, a number of fault outcrops found along the fault scarps of the
244 HPFZ and HHF were excavated and cleaned to observe the fault deformation
245 structures. Seven typical fault outcrops were revealed at Locs 1–7 along the
246 HPFZ and five along the HHF (Locs 8–12). Locs 1–4 were exposed on the
247 boundary between the T3 and T2 terrace risers, and Locs 5–7 on the T2 alluvial
248 riser along the HPF (Figs 7–11), with one trench exposure excavated in the T2
249 terrace riser across the SYF (Fig. 12; see Fig. 2 for the location). Locs 8–12 were
250 exposed on the terrace risers on the eastern side of the Yellow River, and show
251 fault shear zone structures and evidence of Holocene seismic activity. The
252 features found at these various locations are described below (see Figures 2b, 4a,
253 and 6 for locations).
254
255 **4.3.1. The Helanshan Piedmont Fault Zone (HPFZ)**
256 Locs 1–4 were exposed in the southwestern part of the HPFZ on the T3
257 alluvial surface along the boundary between the Helan Mountains and the
258 Yinchuan Graben (Fig. 4). The fault offsets alluvial deposits composed of

interbedded layers of sand–pebbles sourced from the Helan Mountains; these layers were originally titled to the southeast but are now tilted to the northwest (towards the mountains) at angles ranging from 6° to 45° (Figs 7–9). Radiocarbon dating results show that the alluvial deposit surfaces formed during the early Holocene (10,990–11,290 yr BP, CA10 and Ca11; Table 1; Figure 7). The main fault planes strike northeast and dip southeast generally at angles of 50°–60° although locally with angles of <30° (Figs 7–9). The fault zone is 10–20 m wide and is composed of two or three subfaults that form a graben structure (Figs 7–8). The main fault planes occurring in the basement rocks are marked by thin fault gouge zones (3–10 cm thick) and are gray-brown and yellow-brown in color (Fig. 9). Slickenside striations developed on the main fault planes bounded by the fault gouge zone show normal-slip-dominated displacement (Fig. 9d and g).

Locs 5–7 were exposed in the northeastern part of the HPF, in the alluvial sediments on which the Great Wall was built (Figs 10 and 11; see Fig. 5a for locations). The fault has displaced the T1 and T2 alluvial deposits of

275 sand–pebbles sourced from the Helan Mountains, which are overlain by
276 undeformed surface talus deposits (Figs 10 and 11). The main fault planes strike
277 N10–20°E and dip southeast, generally at angles of 40°–60°. The alluvial pebble
278 deposits bounded by the main fault planes have mostly been reoriented to parallel
279 or subparallel to the fault planes, and a wedge structure has formed in the fault
280 deformation zone (Figs 10 and 11). Radiocarbon dating results show that the T2
281 alluvial deposit surfaces formed during the late Holocene (~3300–2300 yr BP,
282 C03–05, C09, and C11; Table 1; Figs 10 and 11), and that the talus deposits
283 overlying the alluvial deposits and covering the fault planes formed at ~2060 yr
284 BP (C10 and C12; Table 1 and Fig. 11). These data indicate that the most recent
285 faulting event occurred at this site between 2300 and ~2060 yr BP.

286 A trench (Trench 1) was excavated at the fault scarp of the SYF on the T2
287 alluvial surface (Fig. 12; see Fig. 2c for the location), the northern wall of which
288 has been reported previously (Deng and Liao, 1996). To identify the
289 paleoseismic events corresponding to those identified from the outcrops, we
290 cleaned, observed, and sketched the southern exposed wall and collected

291 radiocarbon materials for dating. The main fault plane is exposed along the
292 boundary between the gray sand–gravel deposits and the deformed layers of
293 sandy soil and sandy gravel deposits, and is covered by surface talus deposits; the
294 fault plane strikes northeast and dips southeast at an angle of 82° (Fig. 12). On
295 the downthrown side (footwall), the alluvial deposits have also been offset and
296 disturbed by five subfaults, which are found in a deformation zone >5 m wide
297 (Fig. 12c). Radiocarbon dating results show that the alluvial deposits in the lower
298 part of the downthrown side formed during the early Holocene (10,630 ± 60 yr
299 BP, CA06; Table 1; Fig. 12c), and that the upper part of the exposed southern
300 wall in the trench formed at 3960 ±30 yr BP (C07; Table 1; Fig. 12c).
301
302 **4.3.2. The Huanghe Fault (HHF)**
303 Five representative outcrops (Locs 8–12) were found in alluvial deposits
304 sourced from the Yellow River, located along the fault scarp, which is sharply
305 bounded by the western edge of the Ordos Block as shown in high-resolution
306 Google Earth images (Figs 13–15; see Fig. 6 for locations). These outcrops

contain various fault deformation structures of the HHF, as described below.

At Locs 8 and 9, the fault offsets the silt–sand and sand–pebble layers upon distinct fault planes (Figs 13 and 14). The main fault planes strike northeast and dip to the northwest at angles of 32°–56°. Liquefied silt–sand deposits are injected into both the country sand and sand–pebble layers as veins and networks that are then cut by faults (Figs 13b and 14b). The faults and liquefied sand-silt veins occurred in a zone ~5 m wide, in which the alluvial deposit layers are disturbed and tilted to the west at angles of 20°–30° (Fig. 14). Radiocarbon dating results reveal that the disturbed, tilted sand layers formed between 11,050 and 6170 yr BP (CA15 and C12; Table 1; Figs 12b and 14b), and that the upper part of the offset sand layer formed at 2570 ± 30 yr BP (CA14; Table 1; Fig. 14b). From these results, it is inferred that the most recent faulting event occurred during the past ~2570 years. No fresh fault scarp is observed along the HHF because the fault scarp has been strongly eroded, showing either a uniform slope or a step-shaped profile (Figs 6 and 13–15).

At Locs 10 and 11, the fault has displaced sand–silt layers with thin

323 sand–pebble layers that are tilted to the west on the downthrown side at angles of
324 40°–50° (Fig. 15). At Loc 12, a ~15-m-wide graben structure is formed within
325 the fault zone (Fig. 13c), in which the sediment layers have been disturbed and
326 tilted towards the central part of the graben. The tilting of the alluvial deposit
327 layers on the downthrown side, the fault structural features, and the graben
328 structure together indicate that normal faulting occurred in an extensional
329 environment along the HHF, similar to that along the HPFZ in the western
330 marginal zone of the Yinchuan Graben.
331

332 **5. Discussion**

333 **5.1. The seismogenic fault of the 1739 M ~8.0 Pingluo earthquake**

334 Previous studies have reported that the HPFZ was the source seismogenic
335 fault that triggered the 1739 M ~8.0 Pingluo earthquake, based on the apparent
336 offset of the Great Wall (He, 1982; Liao and Pan, 1982; Deng et al., 1984; Zhang
337 et al., 1986; Deng and Liao, 1996). However, our recent study demonstrates that
338 the Great Wall is not offset by faulting along the HPF but was built on the fault

339 scarp developed on the alluvial surfaces (Lin et al., 2013). Based on historical
340 records, the strongest seismic intensity of up to X–XI (on the Chinese XII-point
341 seismic intensity scale) is inferred to be distributed in the central-eastern area
342 around the inferred Yinchuan–Pingluo Fault and the HHF (Fig. 1b; Bai et al.,
343 2005). Historical records made within three weeks of the 1739 earthquake
344 document that in the zone of seismic intensity X–XI, buildings were almost
345 completely destroyed and most people died, and that the intense ground
346 deformation included subsidence of 2–3 m over a wide area, liquefaction, and
347 numerous surface fissures in the area around the Yinchuan–Pingluo and Huanghe
348 faults (Bai et al., 2005). In contrast, the seismic intensity in the Helan Mountains
349 piedmont area along the Luhuatai and Helanshan Piedmont faults during the
350 1739 earthquake was less than VI–VII, leaving buildings only slightly damaged
351 and resulting in no distinct ground deformation (Zhang et al., 1986; Bai et al.,
352 2005). Historical documents record that temples built ~1000 years ago, namely
353 the 15-floor-high towers (Shuang Towers) (Fig. 16a and b) built on the fault
354 scarp of the HPFZ at the site near Suyukou (see Fig. 1b for locations), were not

355 destroyed during the 1739 earthquake, but that 10-floor-high towers (Chentian
356 Tower and Haibao Tower) (Fig. 16c and d) with similar structures to that of the
357 Shuang Towers built in downtown Yinchuan City were completely destroyed and
358 subsequently rebuilt in the Qing Dynasty (~200–300 years ago). These historical
359 records and the pattern of damage to buildings (including the towers) indicate
360 that the strongest ground motion occurred in the narrow belt of seismic intensity
361 of X–XI on the eastern side of the graben around the Yinchuan–Pingluo and
362 Huanghe faults, and that the zone of weakest seismic intensity (≤VI–VII)
363 occurred in the Helan Mountains piedmont area around the HPFZ (Fig. 1b).
364 The seismic reflection data show that the HHF is a main fault in the graben,
365 in which the HPFZ and the Yinchuan–Pingluo Fault converge into a single fault
366 zone at ~30 km depth in the lower crust (Fig. 1c). As stated above, there are no
367 morphotectonic features such as fault scarps along the Luhuatai and
368 Yinchuan–Pingluo faults. The seismic profiles and geological sections based on
369 drilling data and trench investigations indicate that i) the Luhuatai Fault is a blind
370 fault which is buried at a depth of >25 m under the late Pleistocene silt-sand and

soil layers formed before 124 ka (Wang et al., 2007); and ii) that Yinchuan-Pingluo Fault is mostly buried at a depth of >1.5 m under the Holocene fluviolacustrine deposit layers formed during ~3200-13600 yr BP (Cai et al., 2006; Wang et al., 2007). If the 1739 earthquake was triggered by the Yinchuan-Pingluo Fault or the Luhuatai Fault, a distinct coseismic fault scarp with vertical offset of >2-3m would occur on the alluvial landforms along the faults due to the large magnitude of M~8. However, as stated above, the topographical, geological, and seismic reflection data show that no fault scarp and no vertical offset in the near surface deposit layers can be recognized. These data indicate that no morphogenic faulting event has occurred along these two faults since the formation of alluvial landforms during late-early Holocene, and therefore support our findings that these two faults have been morphogenically inactive during the Holocene. In contrast, the HHF vertically offsets the Holocene terrace risers of the Yellow River by 16–17 m (Figs 6 and 13–15), and the most recent faulting event occurred within the past ~2570 years (Fig. 14), which indicates that morphogenic earthquakes have repeatedly occurred on the

387 HHF.

388 The epicentral locations of recent earthquake sequences indicate that the
389 microearthquakes occurred mainly in the central-southern part of the Yinchuan
390 Graben and between the HPF and HHF (Fig. 17). On the basis of the fault dip
391 angle of ~45° revealed by seismic reflection data (Fig. 1c), we interpret the
392 perspective views of the epicentral distribution in the central-southern parts of
393 the graben as indicting that the recent microearthquakes occurred mainly on the
394 HHF (Fig. 17b and c). Although it is unclear whether the recent earthquakes
395 occurring on the HHF are aftershocks associated with the 1739 M ~8.0 Pingluo
396 earthquake, the epicentral distribution indicates that the HHF is a current main
397 seismogenic fault in the Yinchuan Graben. On the basis of the above discussion,
398 we conclude that the HHF is the most likely seismogenic fault to have triggered
399 the 1739 M ~8.0 earthquake.

400

401 **5.2. Recurrence interval of morphogenic earthquakes and normal slip rates**

402 In previous studies, using the apparent offset of the Great Wall, the

403 conspicuous fault scarps developed on the lower terrace riser were considered to
404 be the coseismic fault scarps that formed during the 1739 earthquake (e.g., Zhang
405 et al., 1986; Deng and Liao, 1996). The recurrence interval of the morphogenic
406 faulting events is inferred to be thousands of years to ten thousand or more years,
407 based on the formation time of the old fault scarps developed on the middle and
408 high terrace risers, as calculated from the fault-scarp diffusion model used by
409 Hanks and Wallace (1985) for the Lake Lahontan shoreline and Beachfront Fault
410 scarps (Zhang et al., 1986). Combining the information on the terrace offset, fault
411 scarp morphology, and ^{14}C ages, Deng and Liao (1996) suggested that four
412 paleoseismic events have occurred along the HPFZ, in 8400, 6300–4600, and
413 2600 yr BP, and in AD 1739 (the M ~8.0 Pingluo earthquake). These estimates
414 are based on the idea that the apparent offset of the Great Wall was caused by the
415 1739 Pingluo earthquake and is considered to be the most recent morphogenic
416 faulting event along the HPFZ. As documented above, we present evidence that
417 the fault scarps that developed along the HPFZ were not formed by the 1739 M
418 ~8.0 Pingluo earthquake as stated above and reported by Lin et al. (2013);

consequently, the estimates of recurrence interval inferred from the apparent offset event of the Great Wall, as reported in previous studies, are unreliable.

The fault outcrops exposed in the area around the Great Wall show that the surface talus deposits yielding ^{14}C ages of 2070–2060 yr BP and overlying the disturbed and offset alluvial deposits that formed at 2370–2130 yr BP are neither deformed nor offset by faulting (Figs 10 and 11). This constrains a faulting event to between 2370 and 2060 yr BP. Furthermore, field investigations reveal that the T0 alluvial deposits yielding ^{14}C ages of 1660–1510 yr BP are neither deformed nor offset by faulting along the HPFZ (Fig. 5). Accordingly, considering the error range of dating ages, we infer that the most recent morphogenic faulting event occurred along the HPFZ between ~2300 and 1500 yr BP.

The vertical displacements of the T1, T2, and T3 alluvial surfaces measured in situ range from 0.6 to 2.5 m with an average of ~1.6 m, from 3.2 to 11.2 m with an average of 5.2 m, and from 13.5 to 22.0 m with an average of ~18 m, respectively (Table 2). Considering the post formation erosion and collapse of the fault scarp, the offset amount caused by individual faulting events would be

larger than the average offset amount (1.6 m) of the T1 surface. Using a maximum offset of 2–2.5 m on the T1surface measured in situ as a characteristic offset, we infer that the T1, T2, and T3 surfaces have recorded one, two/three, and seven/eight events on the HPFZ, respectively. Therefore, the recurrence interval of morphogenic faulting events during the Holocene is estimated to be ~1500–2000 years for the HPFZ. Considering the two main fault traces of the HPFZ (the HP and SY faults in the southwestern part of the HPFZ, as shown in Figures 1b and 2a), the characteristic offset caused by an individual event would be the total offset on the HP and SY faults, calculated to be ~3–4 m on average. Accordingly, an average normal slip rate of ~2–3 mm/yr is obtained for the HPFZ. Our results show no evidence for a morphogenic earthquake having occurred in the past ~1500–2000 years along the HPFZ, and therefore the HPFZ has the potential to produce such an earthquake in the near future. This conclusion contrasts with previous interpretations of a recurrence interval of large earthquakes of 2300–3300 years (Deng and Liao, 1996) and of thousands of years to ten thousand years (Zhang et al., 1986), which were based on the view

that the latest event of the HPFZ was the 1739 M ~8.0 Pingluo earthquake. As such, it is necessary to reassess the risk of seismic hazards in the densely populated Yinchuan Graben.

In the case of the HHF, the amount of offset cannot be accurately calculated because of the erosion and collapse of the fault scarps developed on the alluvial terrace risers. Using the limited data obtained in this study, we estimate the vertical displacement on the T3 terrace risers to be ≥16 m (Table 2). On the basis of the ^{14}C dating results (~11,000–6100 yr BP, CA15 and C12; Table 1; Figs 13b and 14b) of the alluvial deposits, an average normal slip rate of 1.2–2.5 mm with an average amount of ~2 mm/yr is obtained for the HHF, which is comparable to that of the HPFZ. Given that the characteristic offset amount of ~2–2.5 m produced by an individual faulting event is similar to the offset proposed for the HPFZ, we estimate that six or seven morphogenic faulting events have occurred during the Holocene, indicating an average recurrence interval of ~1500–2000 years, comparable to that of the HPFZ. The similarity on the recurrence interval and slip rate between the HPFZ and the HHF may be

caused by the same strain stress sourced from the lower crust where two faults join into the same fault zone (Fig. 1c).

More work is required on the Huanghe Fault if we are to better understand the deformation characteristics of the source seismogenic fault of the 1739 earthquake and to improve our ongoing assessment of seismic hazard in the densely populated area of the Yinchuan graben, central China.

6. Summary

On the basis of the field investigations completed as part of this study, the following conclusions can be drawn.

1) The Helanshan Piedmont and Huanghe fault zones are the main active normal faults developed along the western and eastern boundaries of the Yinchuan Graben, respectively.

2) The slip rate during the Holocene is estimated to have been ~2–3 mm/yr for both the HPFZ and the HHF.

3) The recurrence interval of large earthquakes is estimated to be ~1500–2000 years for both the HPFZ and the HHF.

4) The HHF is inferred to be the source seismogenic fault to have triggered the 1739 M ~8.0 Pingluo earthquake, and the HPFZ has the potential to produce a large earthquake in the near future.

Our findings differ from those of previous studies, which considered the HPFZ to have been the source seismogenic fault of the 1739 earthquake and which estimated a recurrence interval for morphogenic earthquakes of >2300–3300 years. Therefore, it is necessary to reassess the seismic hazard of the densely populated Yinchun region, central China.

Acknowledgements

We are grateful to Dr. Y. Zhou and an anonymous reviewer for their critical reviews that helped to improve a previous version of this manuscript. We thank G. Rao and W. Kang for his help in the field and M. Wang for helping to complete Figure 17. This work was supported by a Grant-in-Aid for Scientific Research

498 (A) (Science Project No. 23253002 for A. Lin) from the Ministry of Education,
499 Culture, Sports, Science, and Technology of Japan, and partially by a Research
500 Project of the China Geological Survey (Project No.1212011120099 for J. Hu).
501 Data for this paper may be obtained by contacting the corresponding author.
502

503 **References**

504 Bai, M., Jiao, D., 2005. The historical analysis for M ~8 earthquake in 1739 at
505 Yinchuan-Pingluo area. Northwestern Seismological Journal 27, 135–140
506 (in Chinese with English abstract).
507 Cai, C., Meng, G., Du, P., Wang, Y., Liu, B., Shen, W., Lei, Q., Liao, Y., Zhao,
508 C., Feng, S., Zhang, X., Xie, X., 2006. Comprehensive multi-level
509 exploration of buried active fault: an example of Yinchuan buried active
510 fault. Seismology and Geology 28, 536–546 (in Chinese with English
511 abstract).
512 China Earthquake Data Center, 2014. Seismicity catalog of China,
513 http://data.earthquake.cn/data/ (last accessed 20 Dec. 2014).

514 Deng, Q., Wang, Y., Liao, Y., Zhang, W., Li, M., 1984. Colluvial wedges and
515 Holocene active along the range-front fault of Helan Shan. Chinese Science
516 Bulletin 29, 557–560 (in Chinese with English abstract).
517 Deng, Q., You, H., 1985. Fault scarps research and earthquake risk
518 estimation---example in eastern Helanshan fault scarps. Northwestern
519 Seismological Journal 7, 29–38 (in Chinese with English abstract).
520 Deng, Q., Liao, Y., 1996. Paleoseismology along the range-front fault of Helan
521 Mountains, north central China. Journal of Geophysical Research 101,
522 5873–5893.
523 Fairbanks, R. G., 1990. The age and origin of the “Younger Dryas climatic
524 event” in Greenland ice cores. Paleoceanography 5, 937–948.
525 Fang, S., Zhao, C., Chai, C., B. Liu, Feng, S., Liu, M., Lei, Q., Liu, H., 2009.
526 Seismic evidence of crustal structures in the Yinchuan faulted basin.
527 Chinese Journal of Geophysics 52, 1768–1775 (in Chinese with English
528 abstract).
529 Feng, S., Gao, R., Long, C., Fang, S., Zhao, C., Kou, K., Tan, Y., He, H., 2011.

The compressive stress field of Yinchuan graben: deep seismic reflection profile. Chinese Journal of Geophysics 54, 692–697 (in Chinese with English abstract).

Hanks, T.C., Wallace, R. F., 1985. Morphological analysis of the Lake Lahontan Shoreline and Beachfront Fault scarps, Pershing County, Nevada. Bulletin of Seismological Society of America 76, 75, 835–846.

He, S., 1982. On the dislocation of the Great Wall near the Shizuishan City, Nigxia Automous Region. In: The Active Faults in China 151–153, Beijing, Seismological Press.

Jackson, J. A., 1987. Active normal faulting and crustal extension. Geological Society, London, Special Publications 2, 3-17.

Jackson, J. A., White, N.J., 1989. Normal faulting in the upper continental crust: observations from regions of active extension. Journal of Structural Geology 11, 15–36.

Lehman, S. J., Keigwin, L.D., 1992. Sudden changes in North Atlantic circulation during the last deglaciation. Nature 356, 757–762.

546 Li, M., Wan, Z., 1984. Characteristics of the earthquake-generating structures for
547 magnitude 8.0 Pingluo earthquake of 1739 and he process of its preparation.
548 Seismology and Geology 6, 23–28 (in Chinese with English abstract).
549 Liao, Y., Pan, Z., 1982. Dislocation of the Great Wall in the Hongguozigou,
550 Ningxia Autonomous Region. Seismology and Geology 4, 77–79 (in
551 Chinese with English abstract).
552 Liao, Y., Wang, Y., Kui, F., Song, F., Liu, P., 1982. Preliminary study on the
553 range-front fault of Helan Shan. In: The Active Faults in China, p.162–166.
554 Beijing, Seismological Press.
555 Lin, A., Ren, Z., 2009.The Great Wenchuan Earthquake of 2008—A
556 Photographic Atlas of Surface Rupture and Related Disaster, 121p, Springer,
557 Berlin (ISBN: 978-3-642-03758-0).
558 Lin, A., Ren, Z., Jia, D., 2010. Co-seismic ground-shortening structures produced
559 by the 2008 M_w7.9 Wenchuan earthquake, China. Tectonophysics 491,
560 21–34.
561 Lin, A., Rao, G., Hu, J., Gong, W., 2013. Reevaluation of the offset of the Great

562 Wall caused by the ca. M 8.0 Pingluo earthquake of 1739, Yinchuan graben,
563 China. Journal of Seismology 17, 1281–1294.
564 People Network, 2014. 79 large historic earthquakes recorded in Chinese historic
565 documents, http://politics.people.com.cn/GB/80291/7261351.html (last
566 accessed 10 Dec, 2014).
567 Rao, G., Lin, A., Yan, B., Jia, D., Wu, X., 2014. Tectonic activity and structural
568 features of intracontinental active normal faults in the Weihe Graben, central
569 China. Tectonophysics 636, 270-285.
570 Stuiver, M., Reimer, P. J., Reimer, R., 2003. CALIB Radiocarbon Calibration
571 Version 4.4, http://radiocarbon.pa.qub.ac.uk/calib/ (Last accessed, 20 Dec.
572 2014).
573 Wang, Y., Du, P., Lei, Q., 2007. Summary on recent progress of active fault
574 exploration project in Yinchuan City. Technology for Earthquake Disaster
575 Prevention 2, 166-175 (in Chinese with English abstract).
576 Yang, Z., Duan, Y., Wang, F., Zhao, J., Pan, S., Li. L., 2009. Tomographic
577 determination of the deep earthquake faults in Yinchuan basin by using

578 three-dimensional transmission technology. Chinese Journal Of Geophysics
579 52, 2026-2034 (in Chinese with English abstract).
580 Yeats, R., Seih, K., Allen, C., 1997.The Geology of earthquakes, 568p, Oxford
581 University Press, Oxford.
582 Zhang, B., Liao, Y., Guo, S., Wallace, R. E., Bucknam, R. C., Hanks, T. C. 1986.
583 Fault scarps related to the 1739 earthquake and seismicity of the Yinchuan
584 graben, Ningxia Huizu Zizhiqu, China. Bulletin of Seismological Society of
585 America 76, 1253–1287.
586 Zhang, W., Liao, Y., Pan, Z., Song, F., 1982. On the piedmont scarp in alluvial
587 fan of Mt. Helanshan. Seismology and Geology 4, 32–34 (in Chinese with
588 English abstract).
589 Zhao, W., Zhang, X., Sheng, J., Zeng, X., 2007. Research on seismic risk of
590 segments of each active fault located in Yinchuan Basin. Journal of Natural
591 Disasters16, 79-83 (in Chinese with English abstract).
592

593 **Figure captions**

594 Figure 1. Index map showing the tectonic setting and features of the study area.
595 (a) Landsat image showing the location of the study area; (b) geologic
596 map of the study region [modified from Li and Wan (1984) and Lin et al.
597 (2013), and with seismic intensity data from Bai et al. (2005)]; and (c)
598 seismic reflection profile, showing the subsurface geologic structures of
599 the Yinchuan Graben [modified from Fang et al. (2009)]. ATF: Altyn
600 Tagh Fault; KLF: Kunlun Fault; LSTB: Longmen Shan Thrust Belt;
601 GYXF: Ganzi–Yushu–Xianshuihe Fault; Y.R.: Yellow River.

602 Figure 2. Landsat images (a–d) and photographs (e, f) showing the
603 topographical characteristics and distribution of morphotectonic features
604 in the southwestern part of the HPFZ. (a, b) Google Earth images
605 showing the distribution of morphotectonic features of the HP and SY
606 faults developed on the alluvial fans bounded by the piedmont of the
607 Helan Mountains (see Fig. 1b for the location). Black solid squares
608 indicate the sample locations of radiocarbon dating material with the

609 corresponding dating results. P-4 to P-9 indicate the locations of
610 topographical profiles measured in situ. (c) WorldView image showing
611 the fault traces of the SY Fault. (d) Close-up view of the SY Fault shown
612 in (a). Conspicuous fault traces characterized by white-gray lineaments
613 are prominent in the image. (e) Photograph showing the SY and HP fault
614 scarps. (f) Close-up view of the SY fault scarp.

615 Figure 3. Google Earth image (a), topographical division map (b), photograph
616 (c), and topographical profiles (d) showing the tectonic landforms and
617 geometry of the HPF in the area near Suyukou (see Fig. 2a for the
618 location). (a) Google Earth image and (b) corresponding topographical
619 division map of alluvial surfaces and the topographical features of the
620 HPF. The ^{14}C ages indicate that the T2 terrace riser formed between 5040
621 and 4729 yr BP (Ca-02 and Ca-01). (c) Photograph showing the three
622 levels of terrace risers that have been offset by the HPF. (d)
623 Topographical profiles measured in situ [see (c) for locations]. The T1,
624 T2, and T3 terrace risers are vertically offset by 14.3, 4.4, and 1.2 m,

625 respectively.

626 Figure 4. Google Earth images (a, b) and corresponding topographical division
627 map of alluvial surfaces (c) showing the tectonic landforms and geometry
628 of the HPF in the northeastern part of the Yinchuan graben (see Fig. 1b
629 for the location). (a) Google Earth image showing the configuration and
630 deformation features of the HPF in the area near Suyukou (see Fig. 3 for
631 the location). The fault trace shows an irregular lineament along the
632 piedmont of the Helan Mountains, where seven main fault outcrops (Locs
633 1–7) were observed (see text for details). (b) Close-up view of the area
634 around Loc. 1. (c) Topographical division map of alluvial surfaces in the
635 area shown in (b).

636 Figure 5. Topographical map and photograph showing the tectonic landforms
637 and configuration of the HPF in the northeastern part of the study area
638 around the Great Wall (see Fig. 1b for the location). (a) Google Earth
639 image. (b) Topographical division map of alluvial surfaces in the area
640 shown in (a). (c) Photograph showing the fault scarp developed on the

641 alluvial fan, on which the Great Wall was built. (d) Topographical
642 profiles measured in situ [see (b) for locations]. The T1 and T2 terrace
643 risers are vertically offset by 1.0 and 2.2–4.5 m, respectively.

644 Figure 6. Topographical maps showing the tectonic landforms of the Huanghe
645 Fault in the eastern margin of the Yinchuan Graben (see Fig. 1b for the
646 location). (a, b) Google Earth images. (c) Topographical division map of
647 surfaces in the area shown in (b). (d) Topographical profiles measured in
648 situ [see (a) for locations]. The T2 and T3 terrace risers are vertically
649 offset by 9–11 and 16–17 m, respectively.

650 Figure 7. Photograph (a) and corresponding sketch (b) showing the deformation
651 structures of the HPF at Loc. 1 (see Fig. 4 for the location). The alluvial
652 sand–pebble layers are deformed and tilted to the northwest at an angle of
653 ~45° within a graben structure bounded by two faults. Half arrows
654 indicate the movement sense of the fault. ^{14}C ages indicate that the
655 alluvial terrace riser formed between 10,090 and 11,490 yr BP (CA-11
656 and CA-10).

Figure 8. Photographs showing the deformation structures of the HPF at Loc. 2 (see Fig. 4 for the location). (a) Fault outcrop exposed under the fault scarp. (b) Close-up view of (a). The alluvial sand–pebble layers have been deformed by faults and dip to the northwest at an angle of ~25°.

Figure 9. Photographs showing the deformation structures of the HPF. (a–c) Fault outcrop at Loc. 3. (d) Stereo projection of the striations measured on the main fault at Loc. 3. (e, f) Fault outcrop Loc. 4 (see Fig. 4 for the location). (g) Stereo projection of the striations measured on the main fault plane at Loc. 4. The T3 alluvial terrace riser has been offset and tilted to the northwest. Fault gouge zones, 5–10 cm thick, are observed at these two fault outcrops. Striations on the main fault planes at the two locations indicate a normal, slip-dominated sense of movement.

Figure 10. Photograph (a) and corresponding sketch (b) showing the deformation structures of the HPF at Loc. 5 (see Fig. 4 for the location).

Figure 11. Photographs and corresponding sketches showing the deformation structures of the HPF at Locs 6 and 7 in the northeastern area of the

673 graben in the vicinity of the Great Wall (see Fig. 4 for locations). (a, b)
674 Fault outcrop at Loc. 6. (c, d) Fault outcrop at Loc. 7. The alluvial
675 sand–gravel deposits forming a wedge structure and yielding ^{14}C ages of
676 2310–2310 yr BP (samples C9 and C11) have been offset and deformed
677 by faulting, whereas the surface talus deposits yielding ^{14}C ages of
678 2060–2070 yr BP (samples C9 and C11) have been neither offset nor
679 deformed by faulting.

680 Figure 12. Photographs and sketch of Trench 1 (see Fig. 2c for the location). (a)
681 Overview of the fault scarp at the trench site. (b) Exposed trench wall. (c)
682 Close-up view of the deformation zone of the main fault. (d) Sketch of
683 the exposed trench wall of (b).

684 Figure 13. Photographs showing the fault structure of the HHF at Loc. 8 (a, b)
685 and Loc. 11 (c). The alluvial sand–pebble layers have been deformed and
686 a graben structure is bounded by two main faults (c).

687 Figure 14. Photograph (a) and corresponding sketch (b) of the fault outcrop
688 showing the fault structure of the HHF at Loc. 9. The alluvial sand–gravel

deposits containing carbonate materials yielding ^{14}C ages of 2570 and 6170 yr BP (CA12 and CA14 samples) have been offset and deformed by faulting. The silt–sand deposits have been liquefied and injected into the country alluvial deposits and in turn have been cut by faulting.

Figure 15. Photographs and corresponding sketches of fault outcrops showing the fault structure of the HHF at Loc. 10 (a–c) and at Loc. 11 (d–f). The fault scarps have been eroded and alluvial sediment layers have been tilted towards the downthrown side at an angle of 30°–45°.

Figure 16. Photographs showing the locations and situation of towers built ~1000–1200 years ago in the Yinchuan Graben. (a, b) The 15-floor-high towers (Shuang Towers) were built ~1200 year ago on the uplifted side of the fault scarp of the HPFZ at the site near Suyukou (see Fig. 1b for the location), and were not destroyed during the 1739 earthquake, which were rebuilt several times in the Qing Dynasty (~200–300 years ago). (c, d) The 10-floor-high towers of Chentian Tower and Haibao Tower, which have similar structures to that of the Shuang Towers, were built in

705 downtown Yinchuan City ~1000 years ago and were completely

706 destroyed during the 1739 earthquake and later rebuilt in the Qing

707 Dynasty.

708 Figure17. Epicentral distribution of instrumentally recorded earthquakes (1.0 ≤

709 M ≤ 5.0). (a) Plan-view map. (b) Perspective view of the central part

710 (Profile I–I') of the Yinchuan Graben towards the northeast, showing

711 major faults and instrumentally recorded seismicity. (c) Perspective view

712 of the southern part (Profile II–II') of the Yinchuan Graben towards the

713 northeast, showing the major faults and instrumental record seismicity.

714 Earthquakes recorded from 1970–2014 were obtained from the seismicity

715 catalog (China Earthquake Data Center, 2014).

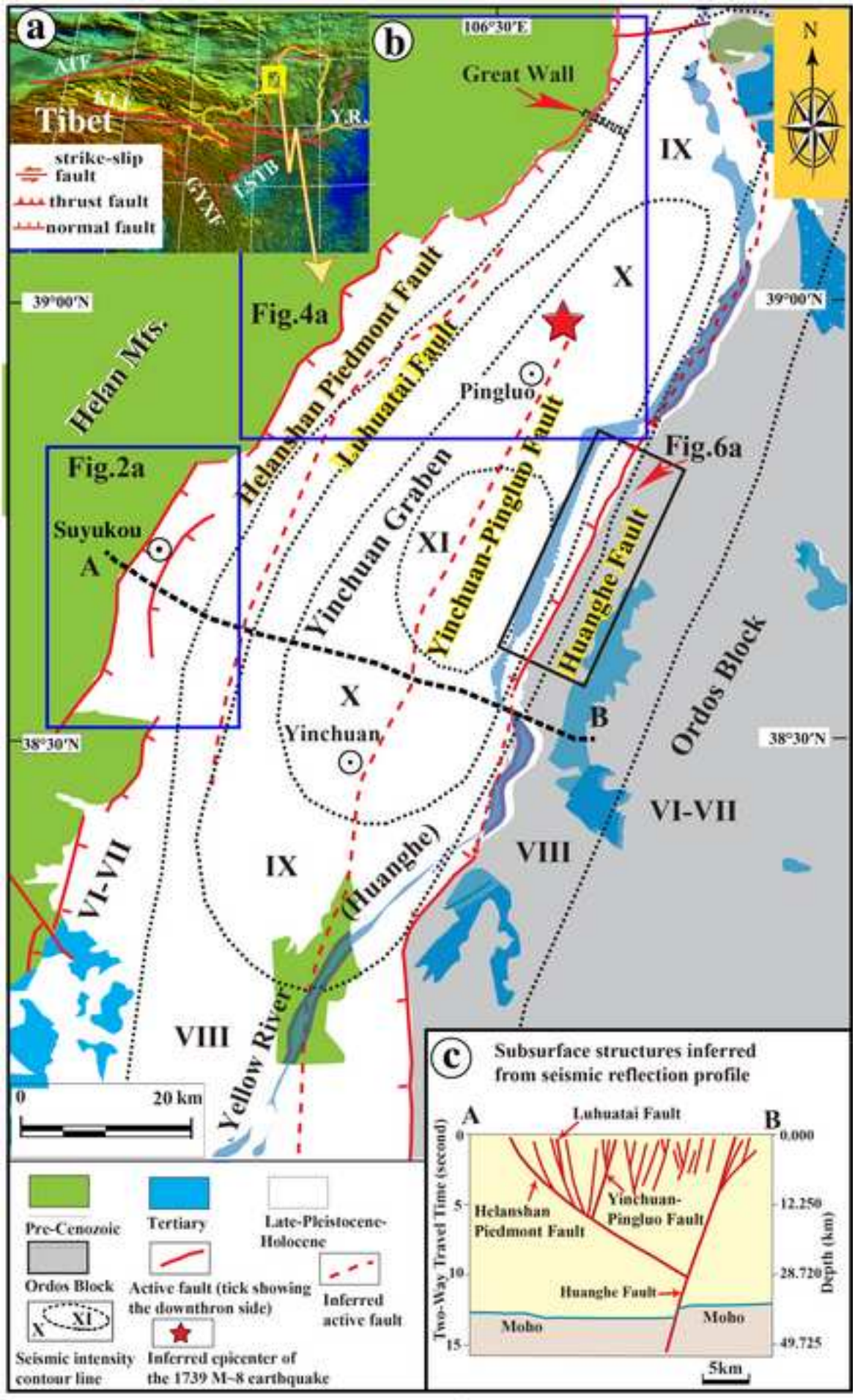

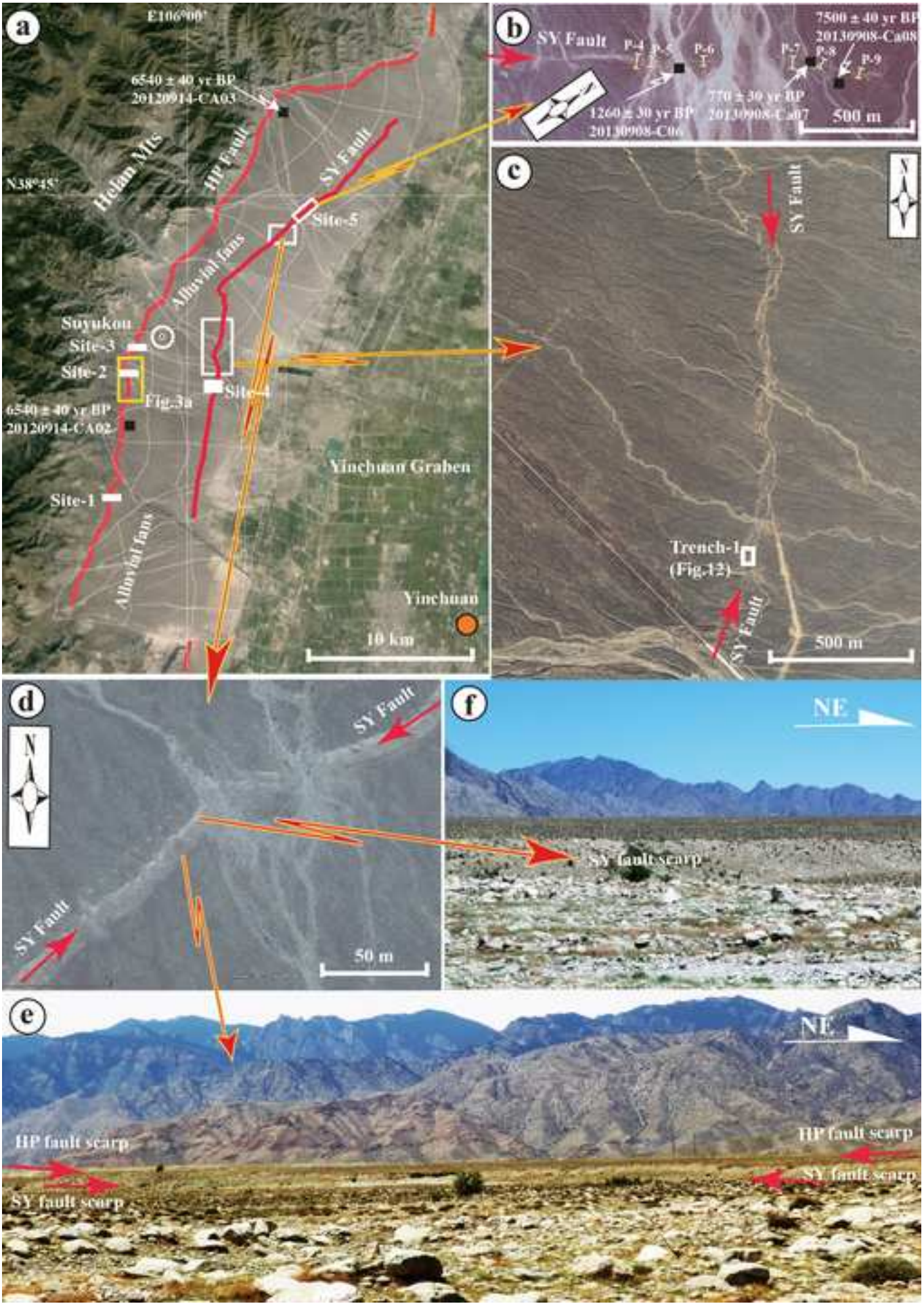

Figure3

Click here to download high resolution image

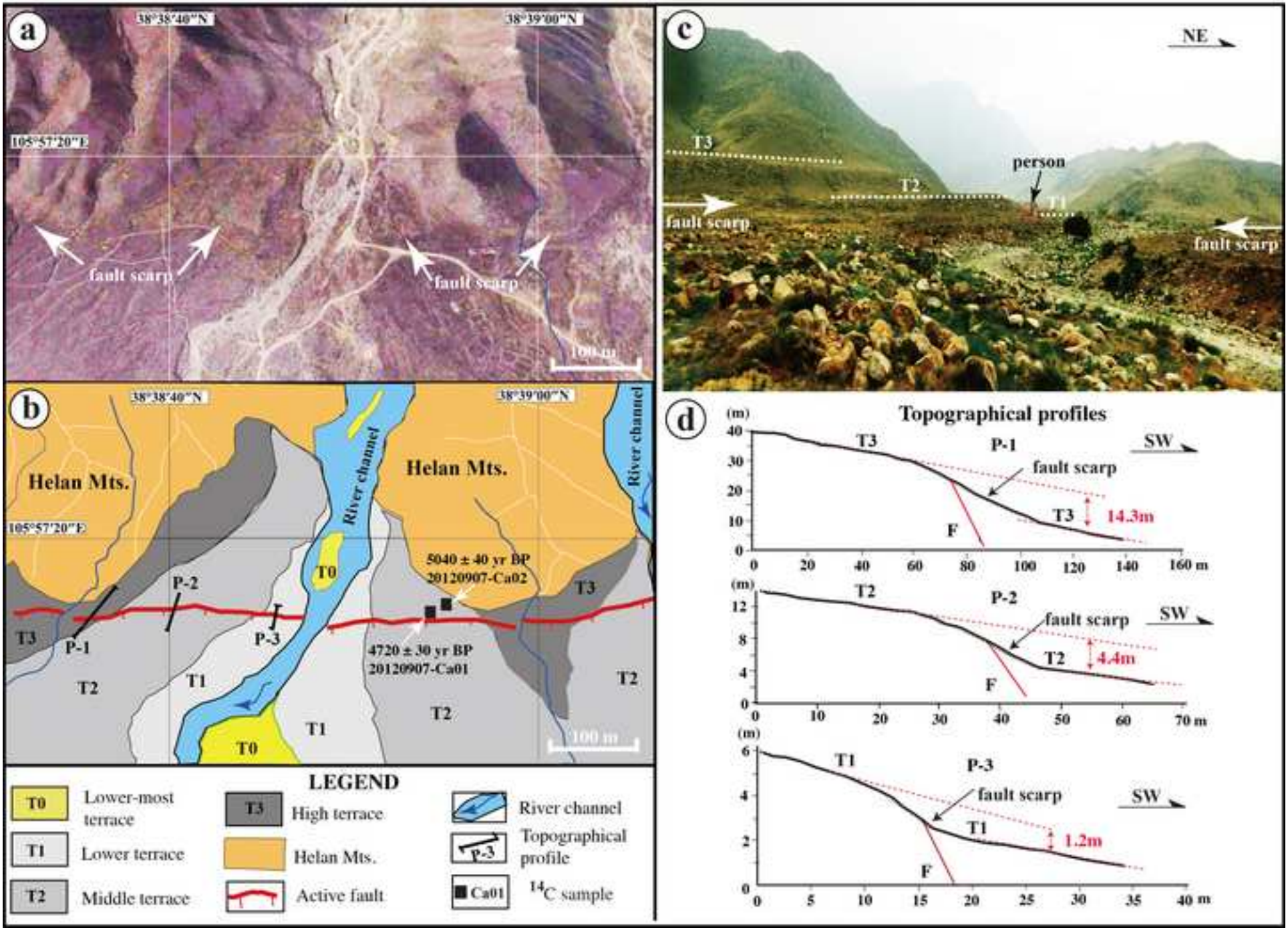

Figure4

Click here to download high resolution image

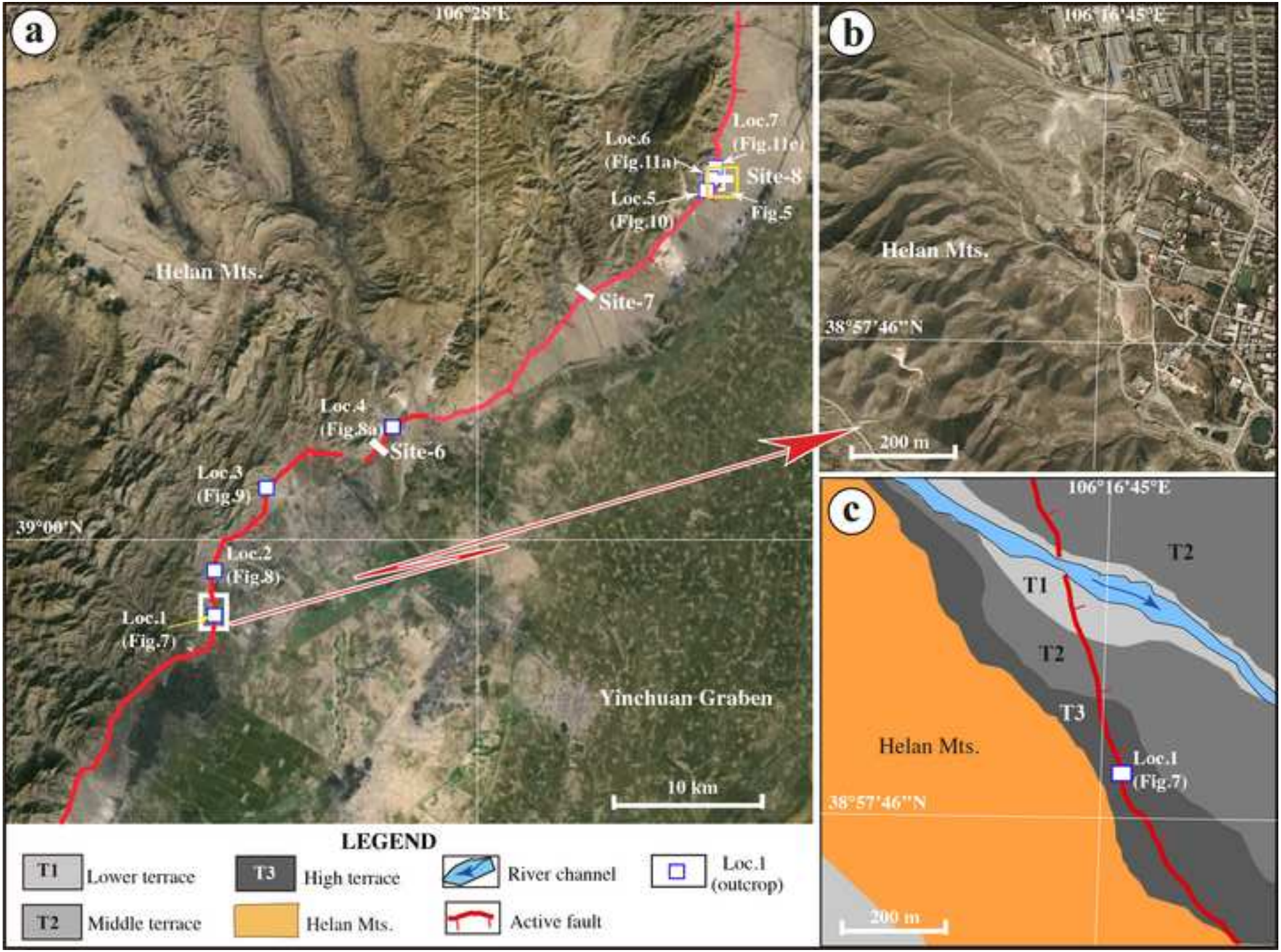

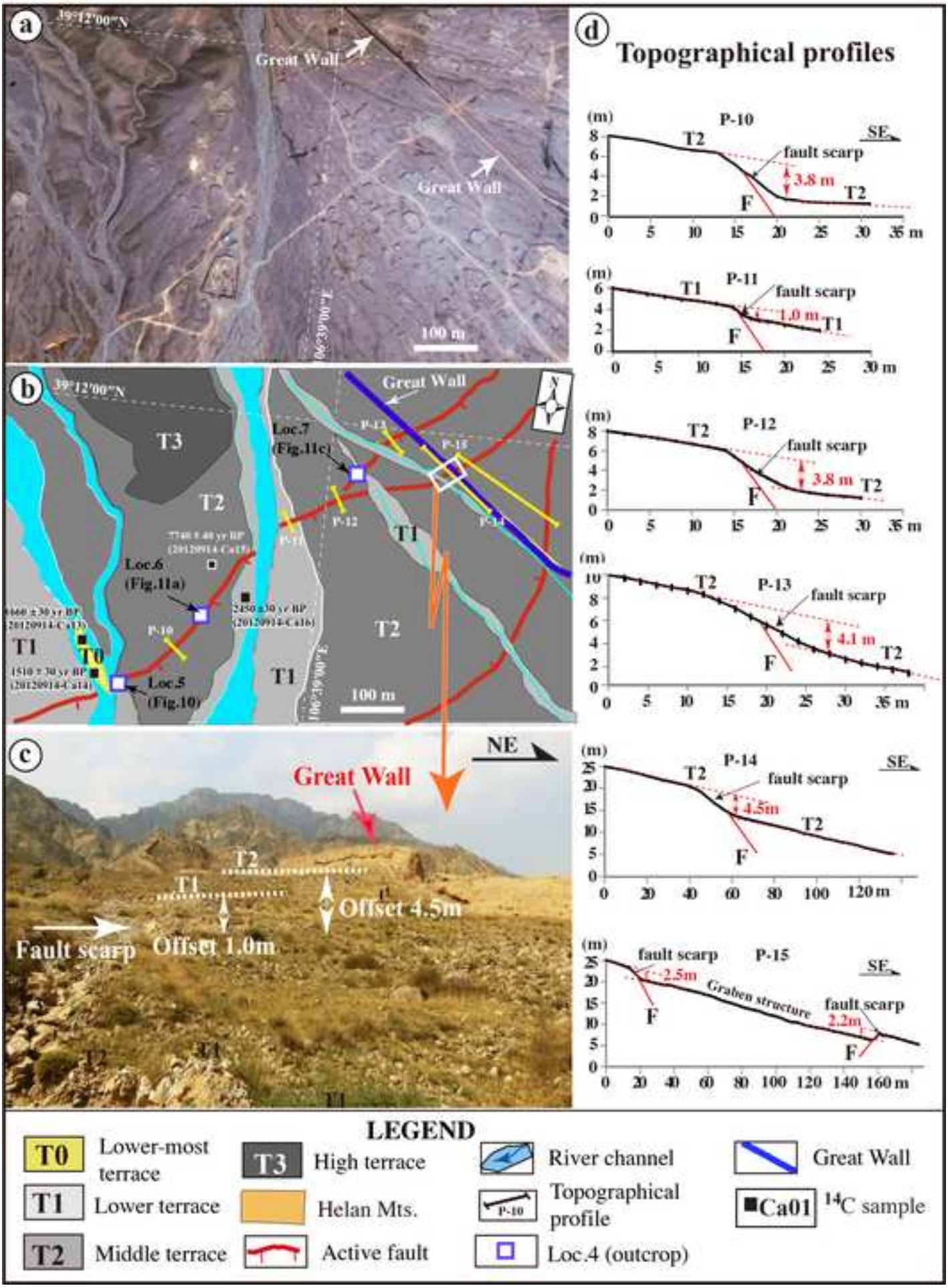

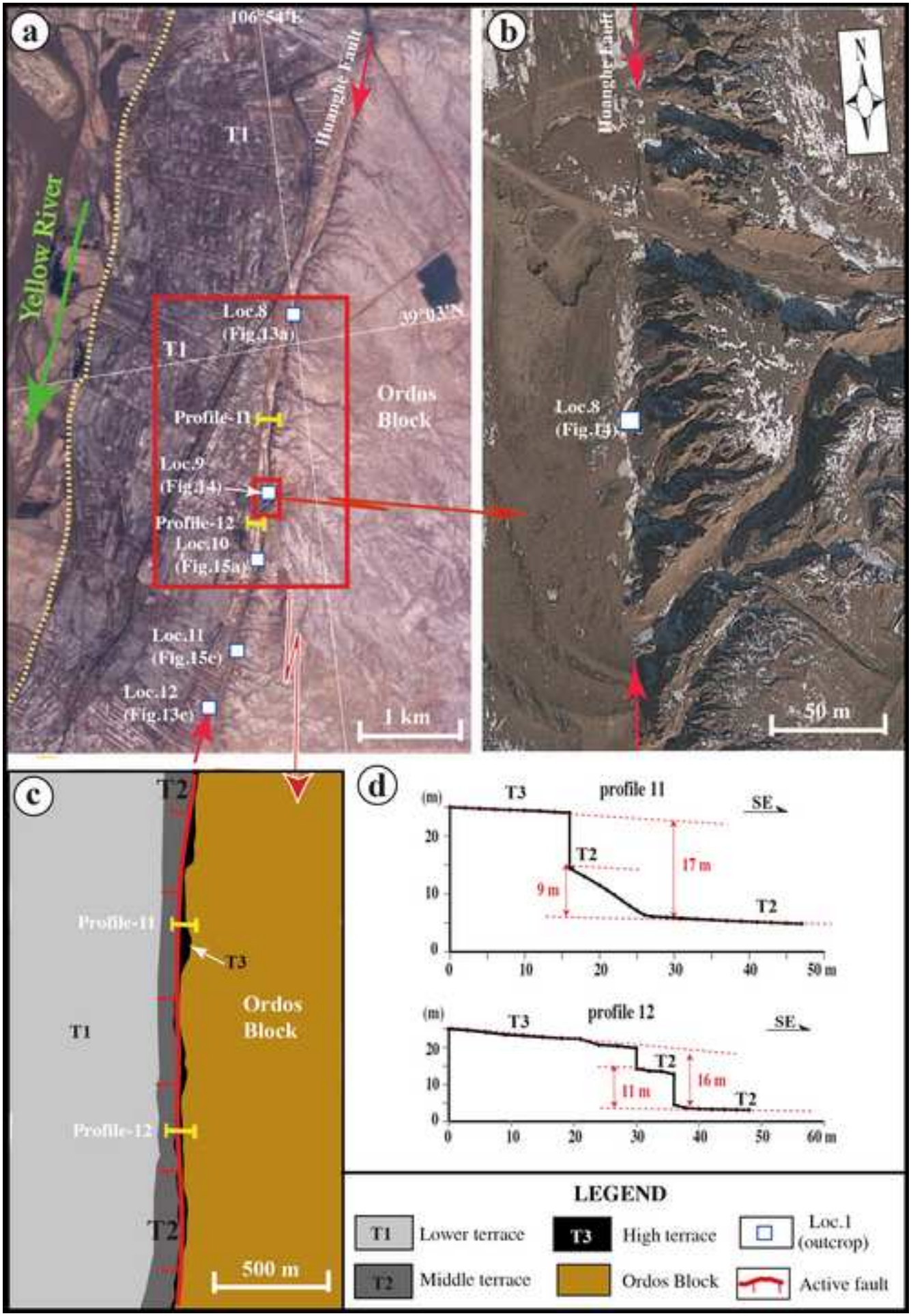

Figure7
Click here to download high resolution image

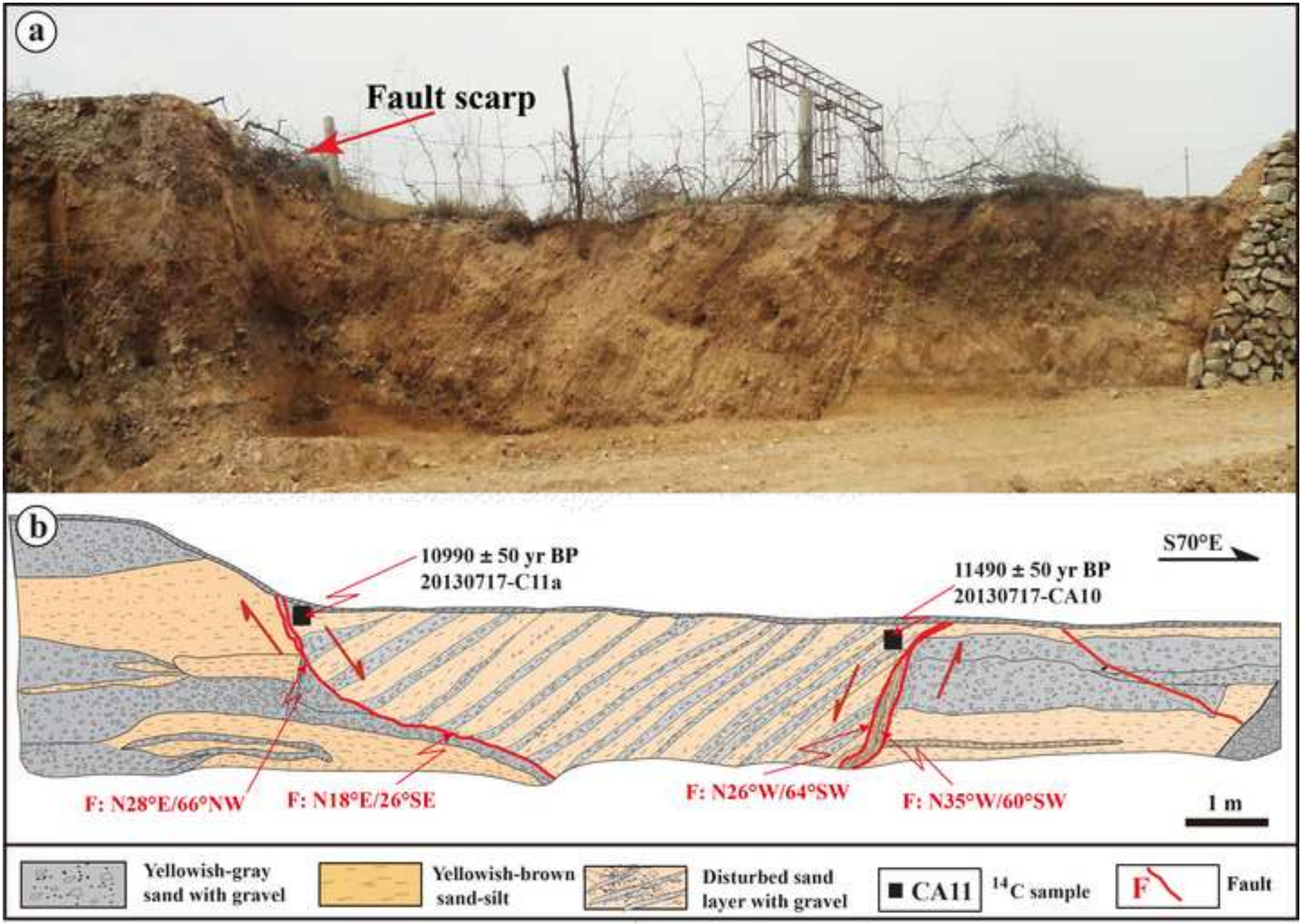

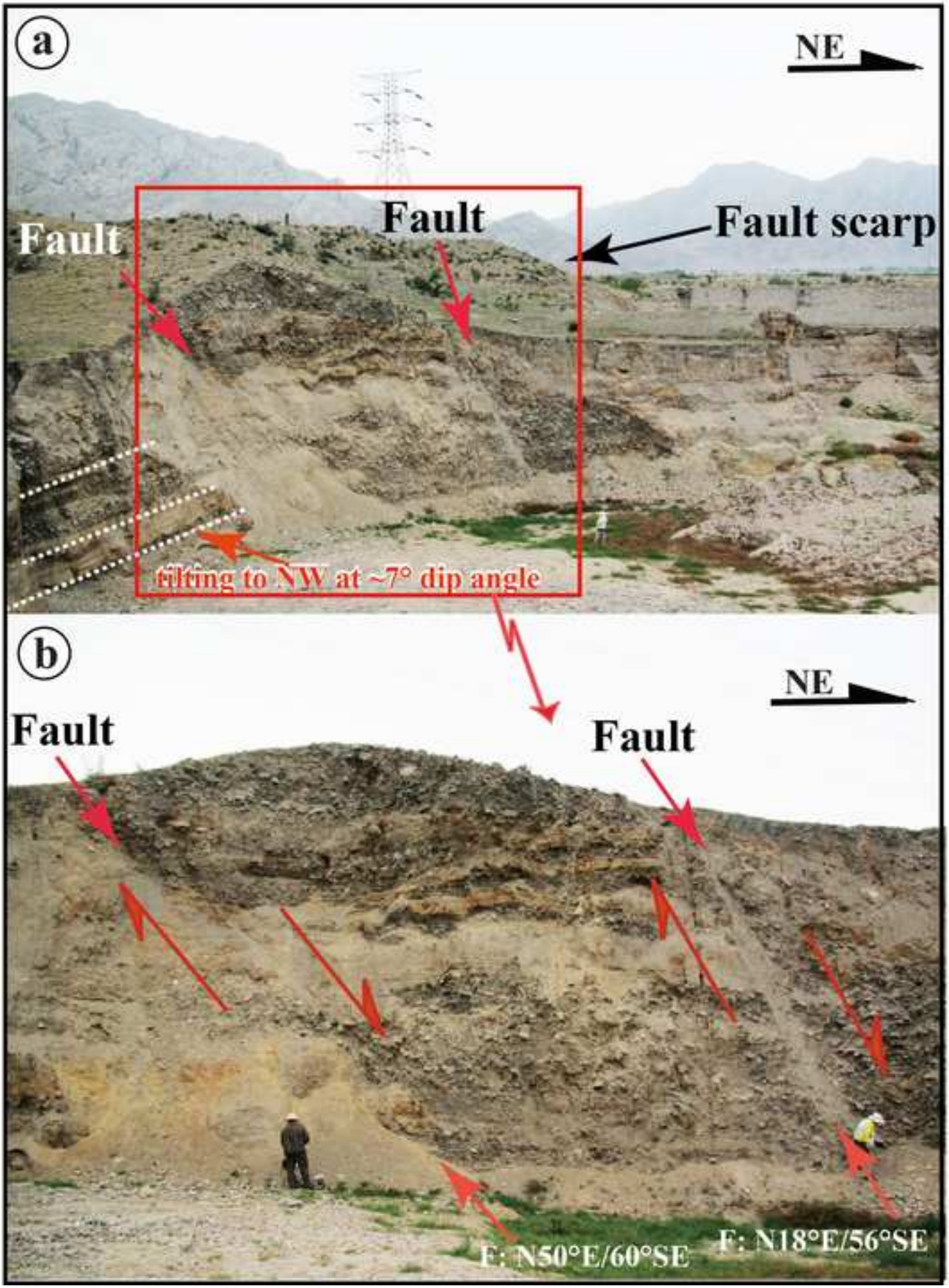

Figure9

Click here to download high resolution image

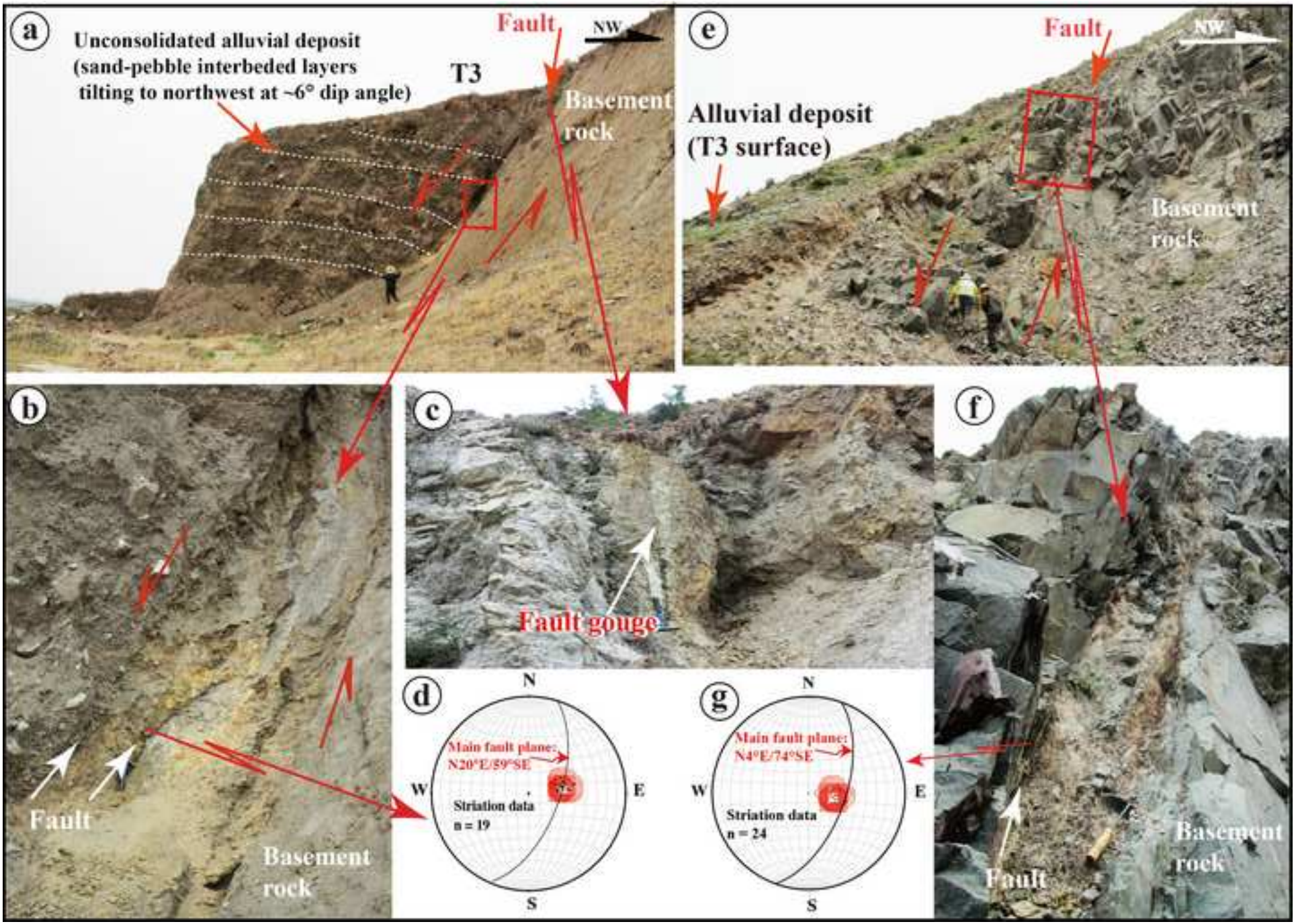

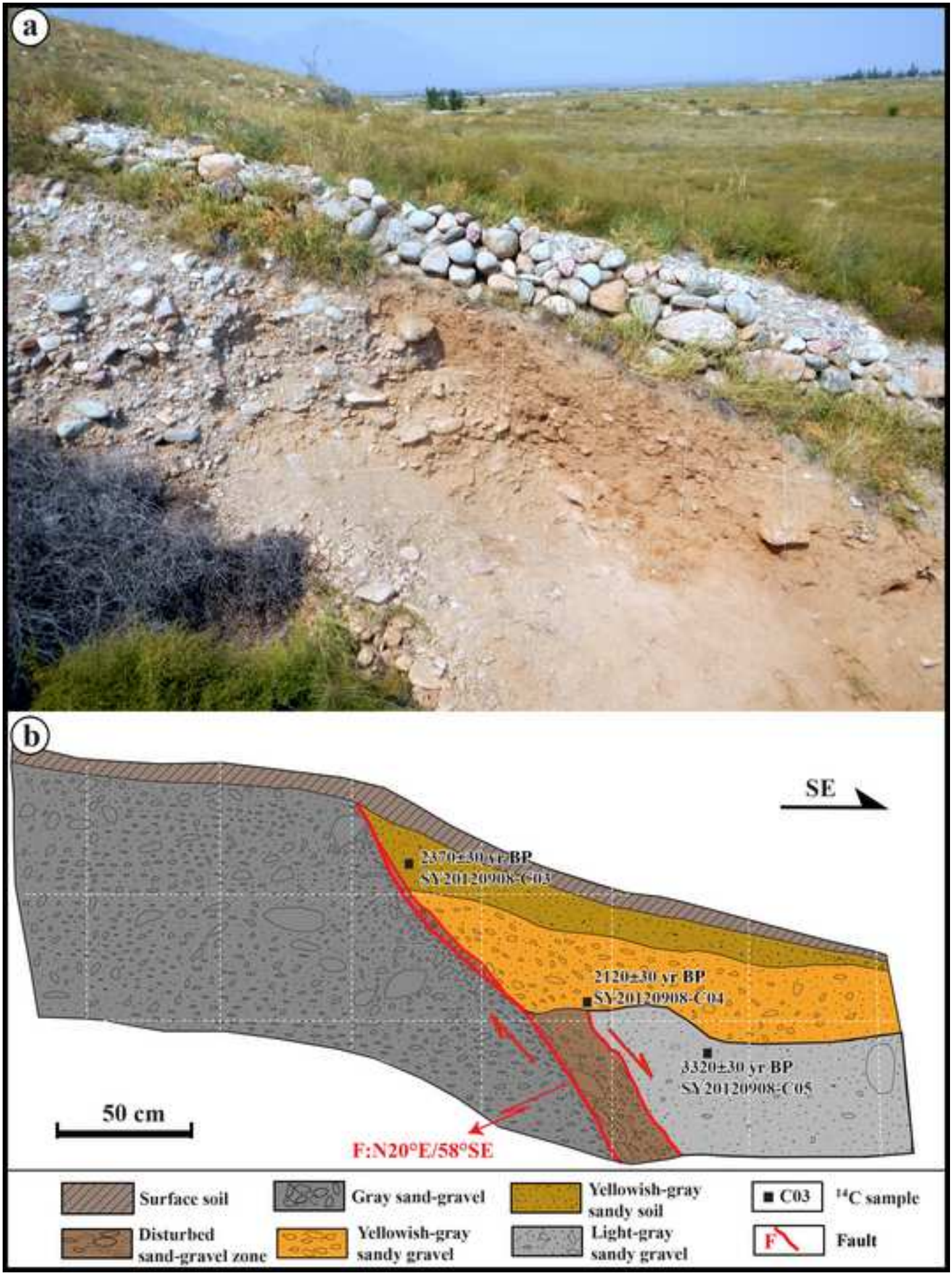

Figure11

Click here to download high resolution image

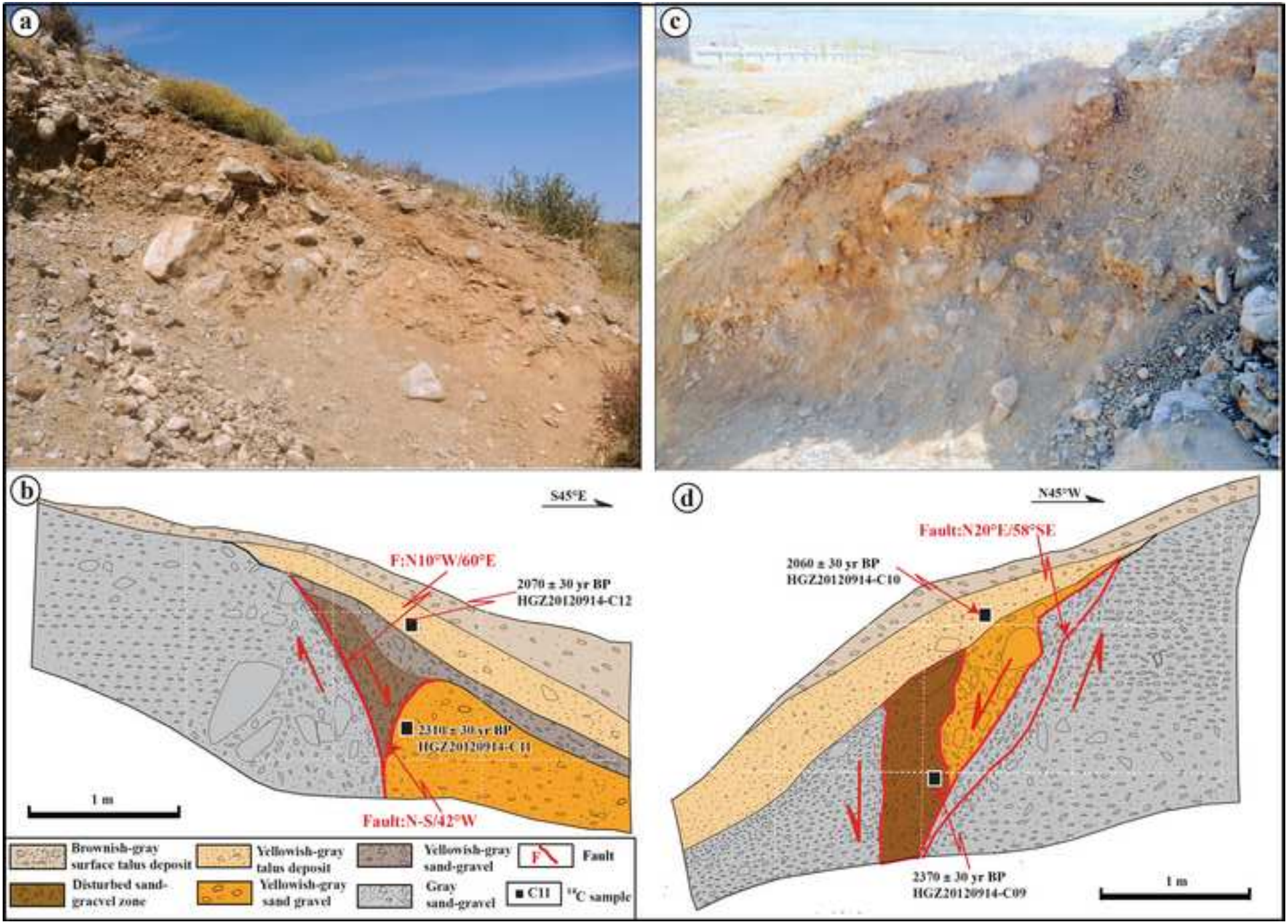

Figure12

Click here to download high resolution image

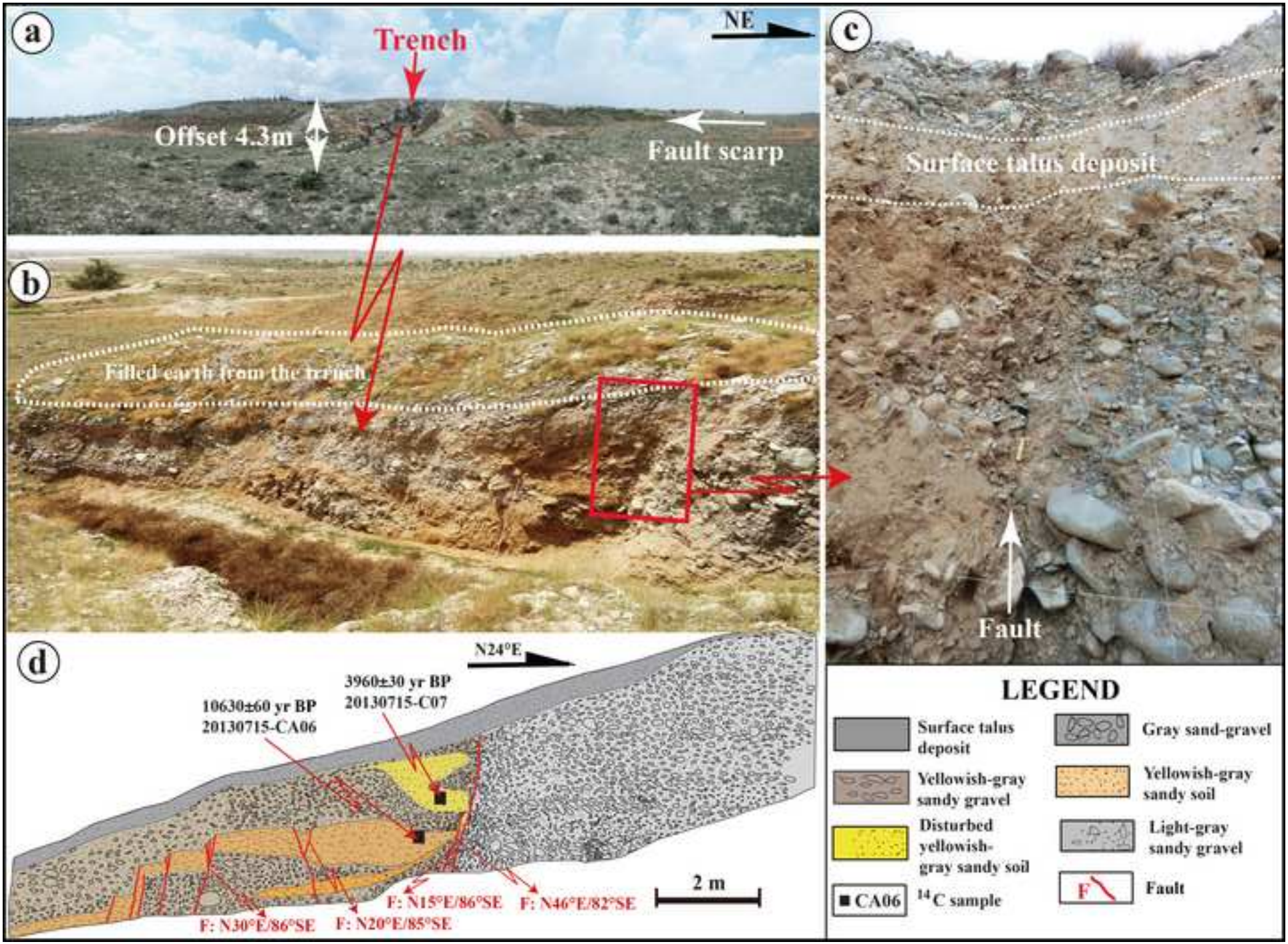

Figure13

Click here to download high resolution image

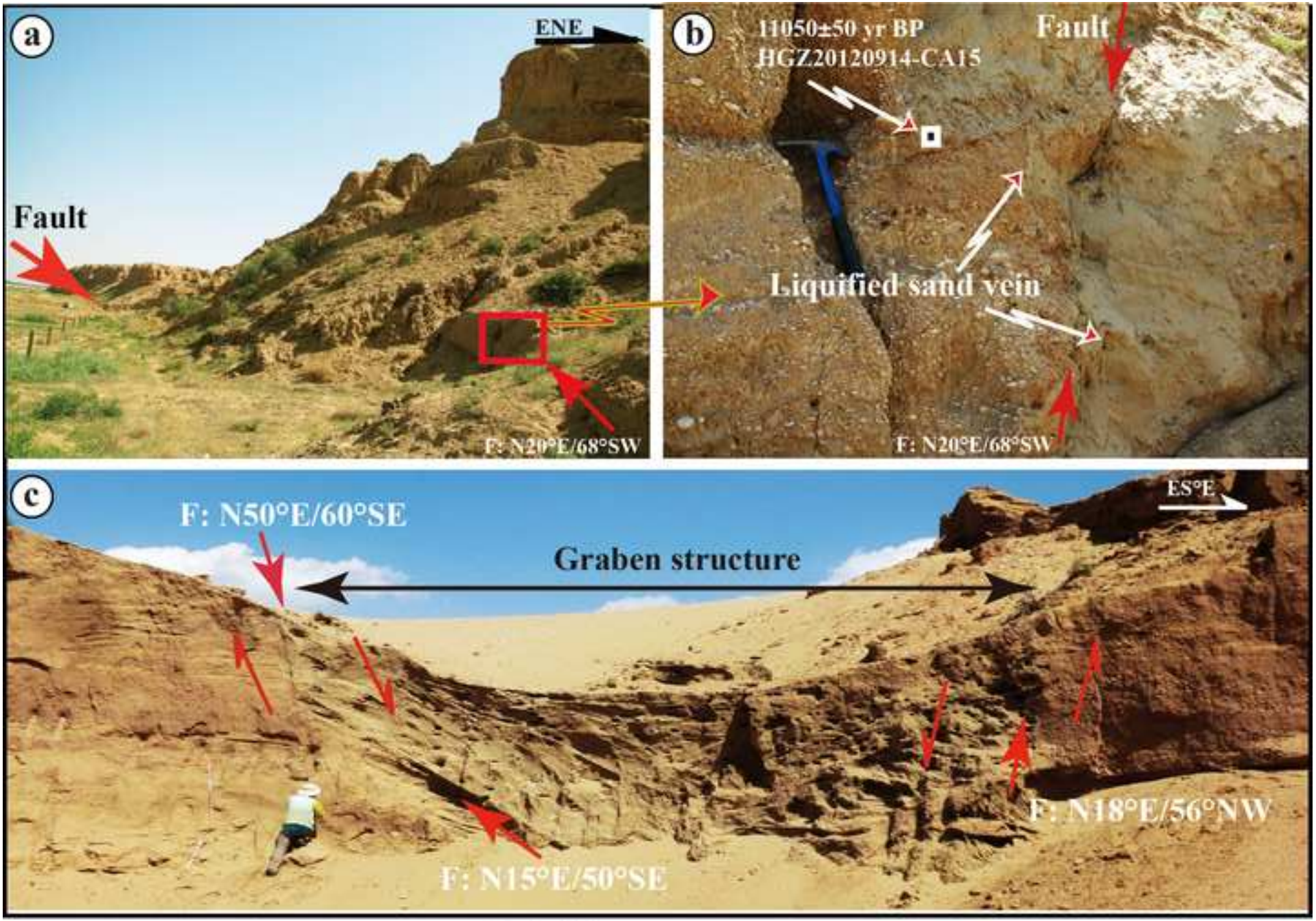

Figure14

Click here to download high resolution image

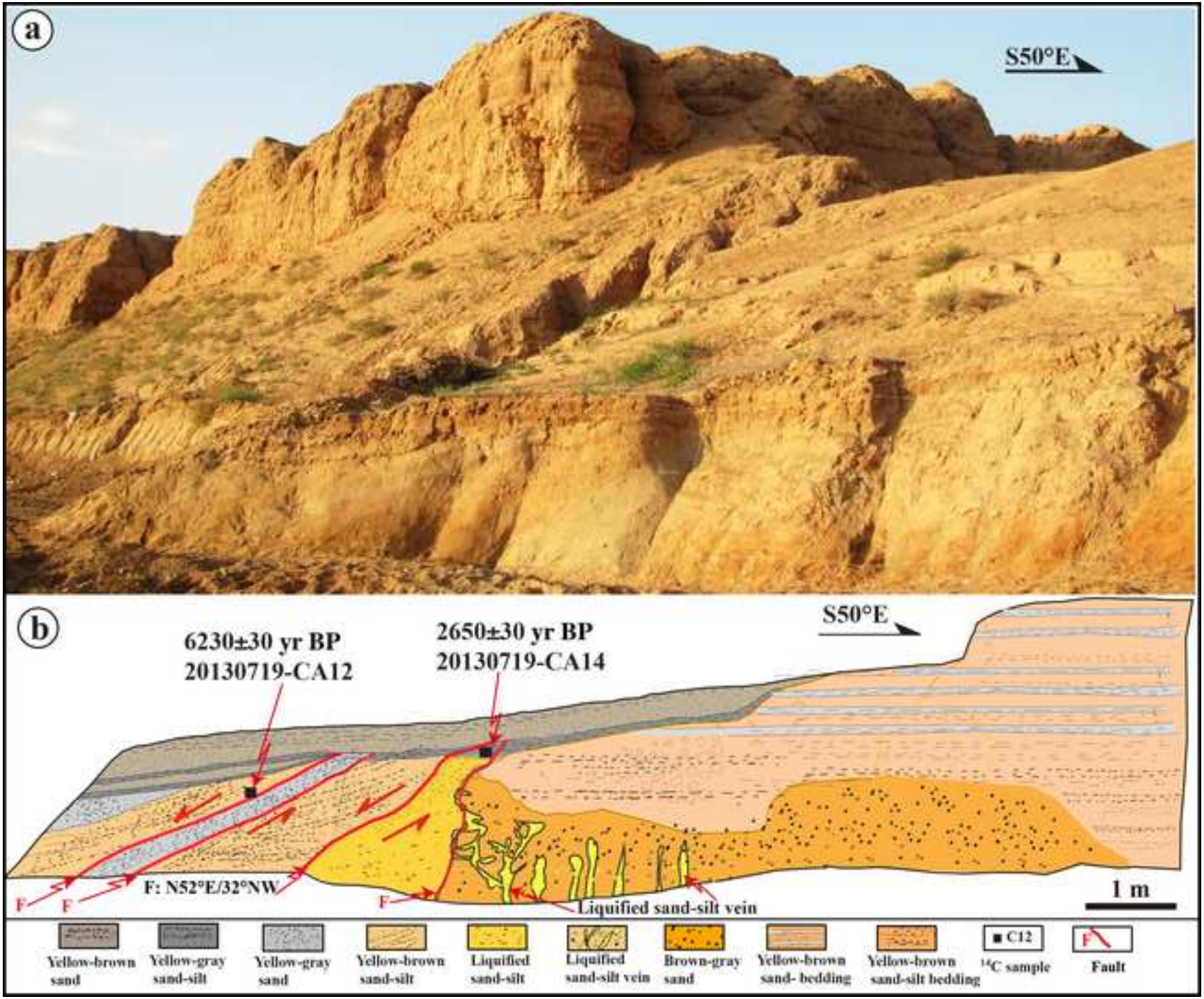

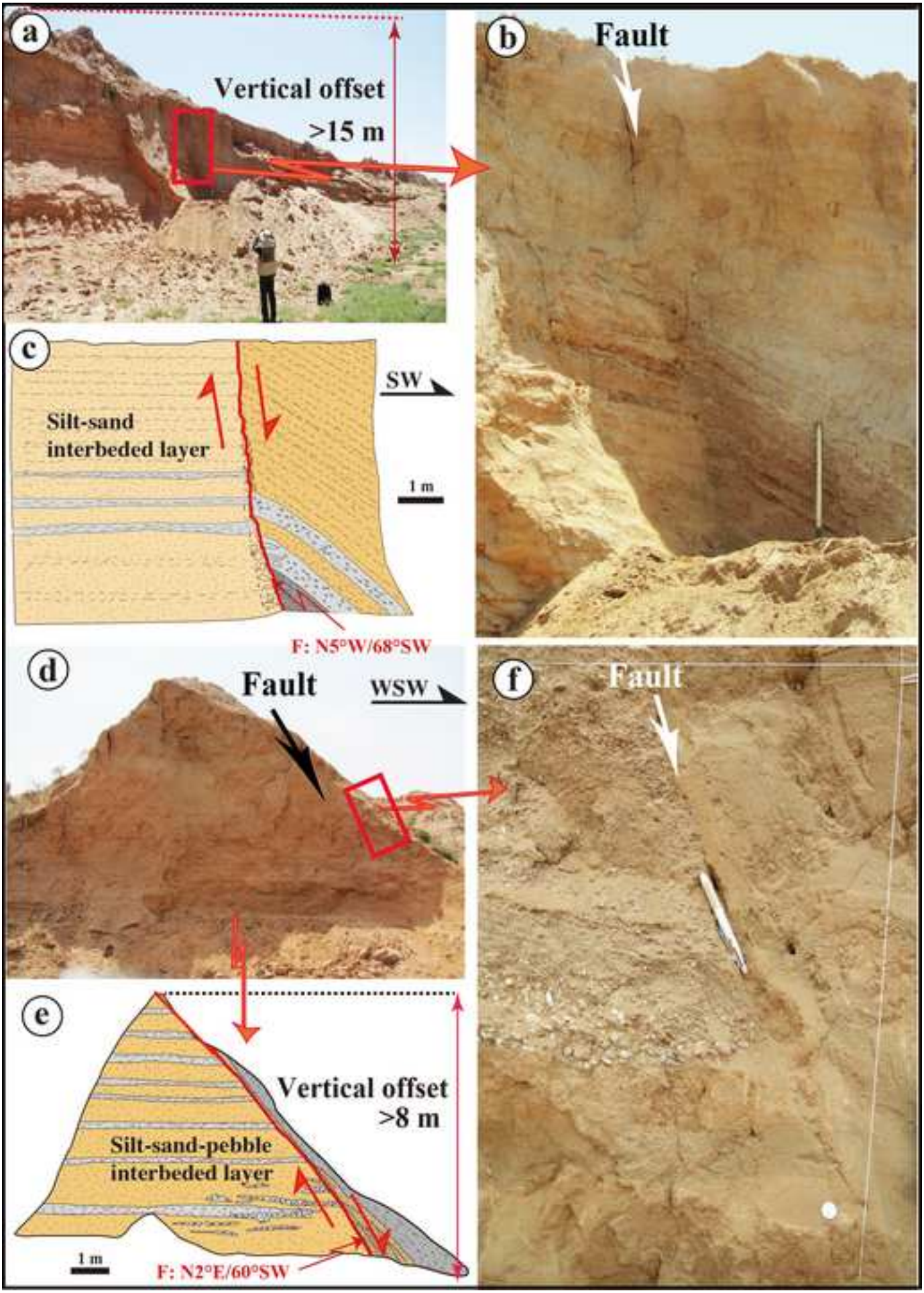

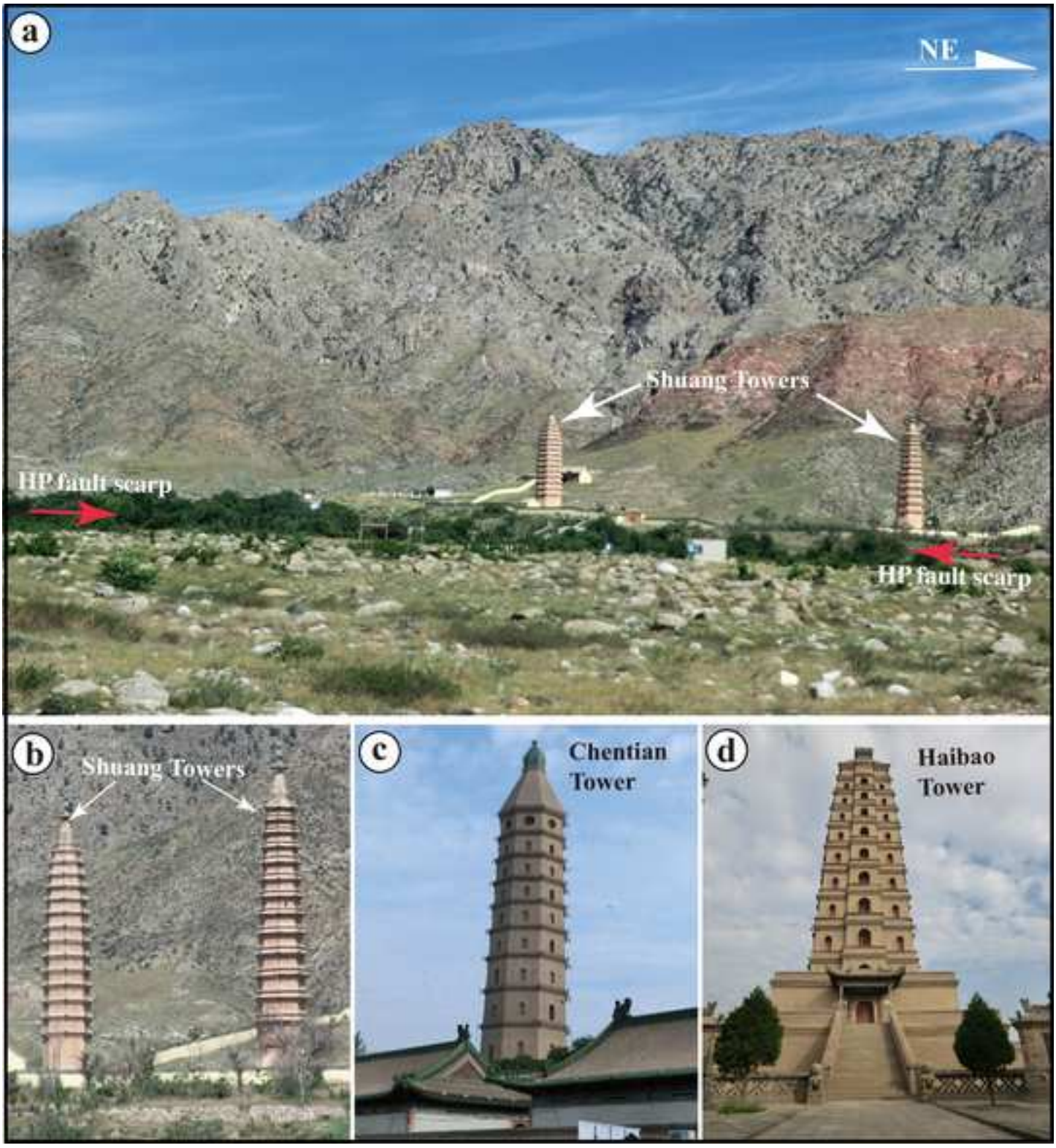

Figure17

Click here to download high resolution image

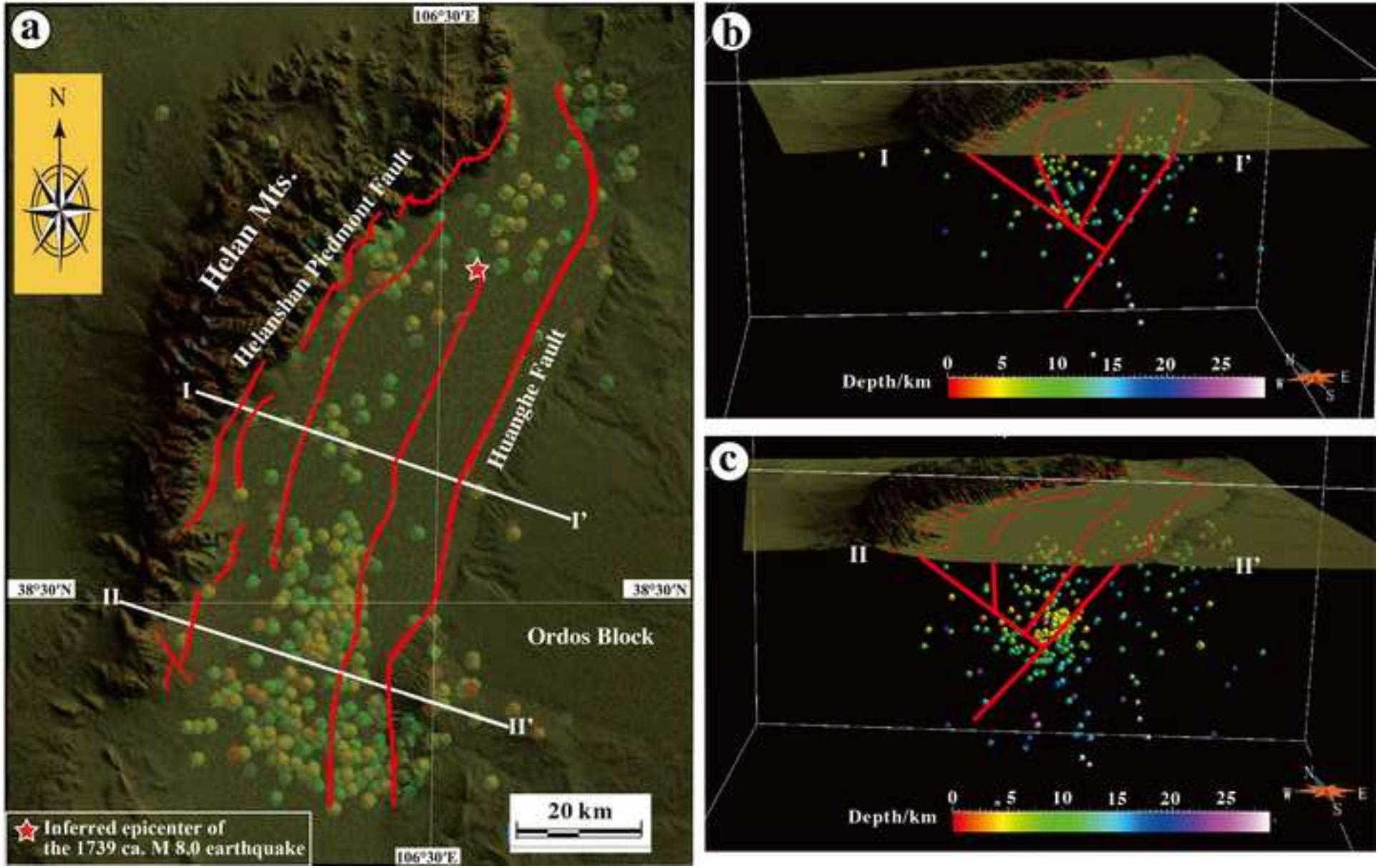

Table 1. Results of ^{14}C dating.

Sample no.	Lab no [a].	Sample material	^{14}C age (yr BP) [b]	Conventional age (yr BP) [c]	2σ calendar age [d]	Sampling location [e]
20120908 Ca01	Beta-335891	car.	4,440 ± 30	4720 ± 3	BC3126-3007	T2 (Fig. 3b)
20120908 Ca02	Beta-335892	car.	4,730 ± 30	5040 ± 30	BC3634-3552	T2 (Fig. 3b)
20120908 C03	Beta-335893	organic soil	2,330 ± 30	2370 ± 30	BC435-360	T2 (Fig. 10b)
20120908 C04	Beta-335894	organic soil	2,060 ± 30	2120 ± 30	BC169-AD3	T2 (Fig. 10b)
20120908 C05	Beta-335895	organic soil	3,220 ± 30	3320 ± 30	BC1535-1425	T2 (Fig. 10b)
20120911 C06	Beta-335896	car.	930 ± 30	1260 ± 30	BC1026-1064	T0 (Fig. 2b)
20120911 C07	Beta-335897	car.	420 ± 30	770 ± 30	BC1421-1498	T0 (Fig.2b)
20120911 C08	Beta-335898	car.	7,220 ± 40	7500 ± 40	BC6126-6013	T2 (Fig. 2b)
20120914 C09	Beta-335899	organic soil	2,240 ± 30	2370 ± 30	BC323-205	T2 (Fig. 11d)
20120914 C10	Beta-335900	organic soil	2,010 ± 30	2060 ± 30	BC60-AD65	Talus (Fig. 11d)
20120914 C11	Beta-335901	organic soil	2,220 ± 30	2310 ± 30	BC374-203	T2 (Fig. 11b)
20120914 C12	Beta-335902	organic soil	1,990 ± 30	2070 ± 30	BC48-AD71	Talus (Fig. 11b)
20120914 Ca13	Beta-335903	car.	1,350 ± 30	1660 ± 30	BC638-712	T0 (Fig. 5b)
20120914 Ca14	Beta-335904	car.	1,220 ± 30	1510 ± 30	BC762-887	T0 (Fig. 5b)
20120914 Ca15	Beta-335905	car.	7,430 ± 40	7770 ± 40	BC6395-6230	T2 (Fig. 5b)
20120914 C16	Beta-335906	organic soil	2,400 ± 30	2450 ± 30	BC543-399	T1 (Fig. 5b)
20130714-CA02	Beta-359857	car.	6530 ± 40	6580 ± 40	BC5562-5464	T2 (Fig. 2a)
20130714-CA03	Beta-359858	car.	6580± 30	6540 ± 30	BC5571-5478	T2 (Fig. 2a)
20130715-CA06	Beta-359859	car.	10570 ± 50	10,630 ± 50	BC10718-10467	T3 (Fig. 12b)
20130715-C07	Beta-359860	organic soil	3870 ± 30	3960 ± 30	BC2464-2479	T2 (Fig. 12b)
20130717-CA10	Beta-359861	car.	11460± 50	11,490± 50	BC11482-11236	T3 (Fig. 7b)
20130717-C11a	Beta-359862	organic soil	10970 ± 50	10,990 ± 50	BC11030-11772	T3 (Fig. 7b)
20130719-CA12	Beta-359863	car.	6170 ± 30	6230 ± 30	BC5216-5033	Trench 1 (Fig. 12b)
20130719-CA14	Beta-359864	car.	2,570 ± 30	2650 ± 30	BC808-749	T2 (Fig. 12b)
20130720-CA15	Beta-359865	car.	11000 ± 50	11,050 ± 50	BC11054-10783	T3 (Fig. 13b

car.: Carbonate material.

[a] All samples were analyzed at Beta Analytic Inc. USA, via accelerator mass spectrometry (AMS).
[b] Radiocarbon ages were measured using accelerator mass spectrometry referenced to the year AD 1950. Analytical uncertainties are reported at 2σ.
[c] Conventional radiocarbon age was calculated using an assumed delta ^{13}C.
[d] Dendrochronologically calibrated calendar age using Method A from CALIB Radiocarbon Calibration Version 7.0 (Stuiver et al., 2003).
[e] Sampling location: carbonate material was taken from the alluvial sediments under the alluvial surface. T0-T3 surface: Lowermost, lower, midddle, and high alluvial surfaces from the current river channel, see text for details.

Table 2. Amounts of offset of alluvial surfaces. T1, T2, and T3 offset (m) indicates the amounts (m) of offset of the T1, T2, and T3 alluvial surface, respectively.

Table 2a. Helanshan Piedmont Fault (HPF).

Location	T3 offset (m)	T2 offset (m)	T1 offset (m)	Location shown in figure
Site-1	13.5			Fig. 2a
Site-2	20.0	3.8	0.6	Fig. 2a
Site-2	14.3	4.4	1.2	Profiles 1–3 (Fig. 3b-c)
Site-3	15.0		1.4	Fig. 2a
Site-7	16	5.5		Fig. 4a
Site-7	22			Fig. 4a
Site-8	20.0	3.8, 4.1, 3.8, 4.5,	1.0	Profiles 10–15 (Fig. 5)
Average	~17.2	~4.3	~1.1	

Table 2b. Suyukou Fault (SYF).

Location	T3 offset (m)	T2 offset (m)	T1 offset (m)	Location shown in figure
Site-4		5.8		Fig. 2a
Site-4			1.4	Fig. 2a
Site-4		5.9		Fig. 2a
Site-4		5.4		Fig. 2a
Site-5		3.2		Fig. 2a
Site-5		11.2, 6.1	2.5, 2.4, 2.1,	Profiles 4–8 (Fig. 2b)
Site-5		5.2		Profile 9 (Fig. 2b)
Average		6.1	2.1	

Table 2c. Huanghe Fault (HHF).

Location	T3 offset (m)	T2 offset (m)	T1 offset (m)	Location shown in figure
Locs 8-9	17			Profile 11 (Fig. 6)
Loc 10	16			Profile 12 (Fig. 6
Average	16.5			